
3D Superconducting Transmon Qubit

THESIS

*Submitted in partial fulfillment of the requirements of
BITS F421T, Thesis*

by

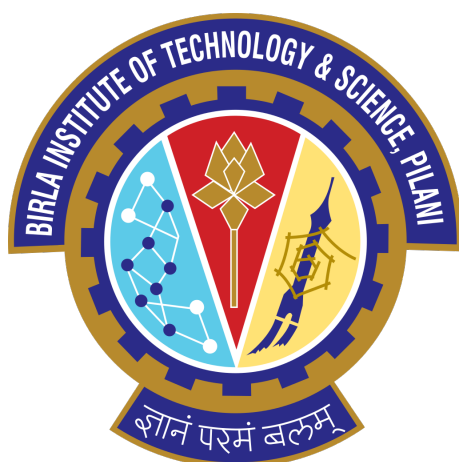
Rohit H Navarathna

ID No - 2013B5TS364G

Under the supervision of

Dr. Vibhor Singh

Assistant Professor, IISc Bangalore



BITS, PILANI –K K BIRLA GOA CAMPUS

Abstract

3D Superconducting Transmon Qubit

by Rohit H Navarathna

Superconducting Qubits are a promising candidate for quantum computing. The use of a high quality 3D superconducting cavity to interact with a Josephson Junction qubit greatly increases it's coherence time. Shunting the Josephson Junction with a large capacitance decreases charge noise exponentially while maintaining the necessary anharmonicity to access only 2 levels of the system. Microwave signals of appropriate frequency can be used to cause Rabi oscillations in the qubit and control it's quantum state. The S_{11} response of the cavity reveals the state of the qubit when they are dispersively coupled. The coherence time and time scales that manipulate the qubit can be estimated using this response.

Acknowledgements

I would like to thank the Academic Research Division in Birla Institute of Technology and Science, KK Birla Goa Campus for giving me this great opportunity.

I would also like to thank my thesis advisor Dr. Vibhor Singh at the Indian Institute of Science, Bangalore. His guidance always helped me in writing this thesis. He consistently allowed this thesis to be my own work, but steered me in the right direction whenever he thought I needed it.

I thank my fellow labmates in the Quantum-NEMS Group: Sudhir Kumar Sahu, Sourav Majumder, Soumya Ranjan Das, Dr. Bindumalini Gunupudi and Soma Mishra for the stimulating discussions and the knowledge they shared with me.

Last but not the least, I would like to thank my family, especially my parents for supporting me throughout this thesis and my life.

Contents

Abstract	i
Acknowledgements	ii
1 Introduction	1
2 Microwave Resonators	2
2.1 Theory	2
2.1.1 Waveguides	2
General Waveguide	2
Rectangular Waveguide	5
2.1.2 Rectangular Waveguide Resonators	8
2.1.3 Coupling to an External Circuit	12
2.2 Experiment	13
3 Superconducting Qubit Theory	19
3.1 Classical LC oscillator	19
3.2 Quantum Electrical Circuits	20
3.2.1 Quantum LC oscillator	20
3.2.2 Nonlinear Harmonic Oscillator	22
3.3 The Josephson Junction	24
3.4 The Cooper Pair Box	27
3.5 The 3D Superconducting Transmon	31
3.6 Coupling the Transmon to a Resonator	33
3.7 The Bloch Sphere	35
3.8 Dynamics of the Jaynes-Cummings system	37
3.9 Decoherence	42

3.10 Measurement Theory (Dispersive Limit)	43
3.10.1 Single tone measurement	44
3.10.2 Two tone measurement	44
A Calculation of Required Junction Resistance	46
B Time Domain Measurements	48
Bibliography	50

List of Figures

2.1	Waveguide Types	3
2.2	Probe in resonator	12
2.3	External coupling circuit	12
2.4	Aluminium Cavity	13
2.5	External Circuit	14
2.6	Dilution Refrigerator	15
2.7	Quality Factors for different pin lengths	17
2.8	Sample S_{11} fit	18
2.9	Quality Factors for different powers at low temperature	18
3.1	LC oscillator	19
3.2	Harmonic Oscillator Energy Levels	21
3.3	Josephson Junction	24
3.4	Cooper Pair Box circuit	27
3.5	Energy Level for $E_J = 0$	28
3.6	Different E_J/E_C	31
3.7	Transmon Circuit	33
3.8	Bloch Sphere Representation	36
3.9	Qubit Evolution on Bloch Sphere	37
3.10	Dispersive Shift	39
3.11	Measurement Setup	43

List of Tables

List of Abbreviations

AC	Alternating Current
BCS	Bardeen Cooper and Schrieffer
FWHM	Full Width at Half Maximum
HEMT	High Electron Mobility Transistor
QED	Quantum Electro-Dynamics
QND	Quantum Non Demolition
SHO	Simple Harmonic Oscillator
SIS	Superconductor-Insulator-Superconductor
TE	Transverse Electric
TEM	Transverse Electric and Magnetic
TM	Transverse Magnetic
VNA	Vector Network Analyser

Physical Constants

Speed of Light	$c_0 = 2.997\,924\,58 \times 10^8 \text{ m s}^{-1}$ (exact)
Reduced Planks Constant	$\hbar = 1.054\,571\,800 \times 10^{-34} \text{ Js}$
Planks Constant	$h = 6.626\,070\,04 \times 10^{-34} \text{ Js}$
Elementary Charge	$e = 1.602\,176\,62 \times 10^{-19} \text{ C}$
Magnetic Flux Quantum	$\Phi_0 = 2.067\,833\,831 \times 10^{-15} \text{ Wb}$
Boltzmann Constant	$k_B = 1.380\,648\,52 \times 10^{-23} \text{ J K}^{-1}$
Pi	$\pi = 3.141\,592\,653\,59$

List of Symbols

Microwave Resonators

C	Capacitance	F
\bar{E}	Electric Field	V m ⁻¹
\bar{H}	Magnetic Field	T
k	Wave Number	m ⁻¹
L	Inductance	H
Q	Quality Factor	
Q_c	Coupling Quality Factor	
Q_i	Internal Quality Factor	
Q_t	Total (Loaded) Quality Factor	
R	Resistance	Ω
S_{ij}	Scattering Parameter	
v_p	Phase Velocity	m s ⁻¹
Z	Impedance	Ω
α	Attenuation	
β	Propagation Constant	
γ	$\alpha + j\beta$	
ϵ	Electric Permittivity	F m ⁻¹
ϵ_r	Relative Electric Permittivity	
η	Intrinsic Impedance	Ω
κ	Cavity Decay Rate	Hz
κ_e	External Cavity Coupling Rate	Hz
κ_i	Internal Cavity Coupling Rate	Hz

μ	Magnetic Permeability	H m^{-1}
μ_r	Relative Magnetic Permeability	
σ	Electric Conductivity	$\text{S } \Omega^{-1}$
ω	Angular Frequency	rad s^{-1}
ω_0	Resonance Frequency	rad s^{-1}

Superconducting Qubit Theory

a	Annihilation,Amplitude Operator	
a^\dagger	Creation Operator	
C	Capacitance	F
C_c	Coupling Capacitance	F
C_g	Gate Capacitance	F
C_j	Josephson Capacitance	F
C_s	Shunt Capacitance	F
E_C	Charging Energy	J
E_J	Josephson Energy	J
E_n	Energy of n th Energy Eigenstate	J
E_{kin}	Kinetic Energy	J
g	Qubit-Cavity Coupling Coefficient	si
\mathcal{H}	Hamiltonian	J
I	Bias Current	A
I_0	Critical Current	A
I_s	Superconducting Current	A
L	Inductance	H
L_J	Josephson Inductance	H
n_g	Gate Charge Number	si
p	Momentum	kg m s^{-1}
q	Charge	C
T_1	z component Relaxation Time	s
T_2	Transverse Relaxation Time	s

U	Potential Energy	J
$\hat{U}(t)$	Unitary Time Evolution Operator	
V	Voltage	V
V_g	Gate Voltage	V
x	Position	m
Z_0	Characteristic Impedance	Ω
α	Eigenvalue of Coherent State	
α_h	Anharmonicity	J
δ	Superconducting Phase Difference	rad
Δ	Detuning	Hz
σ_-	Qubit Annihilation Operator	
σ_+	Qubit Creation Operator	
σ_z	z -Pauli Matrix	
ϕ	Flux	Wb
ψ_0	Ground State Wavefunction	
ω_0	Resonance Frequency	rad s^{-1}
ω_d	Qubit Drive Signal Frequency	rad s^{-1}
ω_{ij}	$ i\rangle \rightarrow j\rangle$ Transition Frequency	rad s^{-1}
ω_p	Probe Signal Frequency	rad s^{-1}
ω_q	Qubit Transition Frequency	rad s^{-1}
ω_r	Cavity Resonance Frequency	rad s^{-1}
$ e\rangle$	Qubit Excited State	
$ g\rangle$	Qubit Ground State	
$ n\rangle$	n th Number state	
$ \alpha\rangle$	Coherent State with eigenvalue of α	
$ \psi\rangle$	Arbitrary State	

Chapter 1

Introduction

The key to improving computing performance for the past few years has been to reduce the size of the transistors used in the process, but this process cannot continue for much longer since the effects of quantum mechanics will prevent the further reduction of transistor size.

In 1982, Richard Feynman suggested that we could use the effects of quantum mechanics to our advantage and build a "quantum computer". For a few decades, quantum computers were only of theoretical interest. Many quantum algorithms were developed which could perform certain tasks exponentially faster than their classical counterparts.

In 1998, the first Nuclear Magnetic Resonance (NMR) quantum computers were implemented.

Cavity QED, which is the study of light in a superconducting reflective cavity interacting with atoms, can be used for many physical applications including quantum computing and has been studied since the 1940s.

Circuit QED, which is basically cavity QED where superconducting circuits are used instead of a reflective cavity. Microwave photons are used instead of optical light and Josephson Junction s are used instead of atoms. The Josephson Junction s have a transition frequency which is of the same order as microwaves.

This thesis describes the use of a superconducting cavity as a microwave resonator, and discusses it's interaction with an implementation of a qubit, called a transmon.

Chapter 2

Microwave Resonators

2.1 Theory

In most low frequency AC circuits, we are used to transmitting the signal in 2 conductors (or wires). At these frequencies, the wavelength of the signal is very large compared to the length of the conductors, so we assume that the signal is the same as the generator signal at all points in the conductors. In reality, there will be a small phase shift and an amplitude loss between the signal at the signal generator and the other end of the "wires". This phase shift, along with other phenomena can be easily observed at high frequencies.

At high frequencies, the geometry and properties of the material plays an important role in the transmission. The replacement for what we knew as just "wires" are called *Transmission Lines* or *Waveguides*.

2.1.1 Waveguides

There are many different types of waveguides. Some of them are shown in Fig. 2.1. The case we will be dealing with in this thesis pertains to rectangular waveguide.

General Waveguide

Consider a general cross-section of a dielectric surrounded by conductor (can have one more conductor in the dielectric) which continues infinitely along the z axis. We can write down the electric and magnetic fields in the dielectric in phasor domain. We assume that the wave propagates in the z -axis and has an $e^{j\omega t}$ dependence.

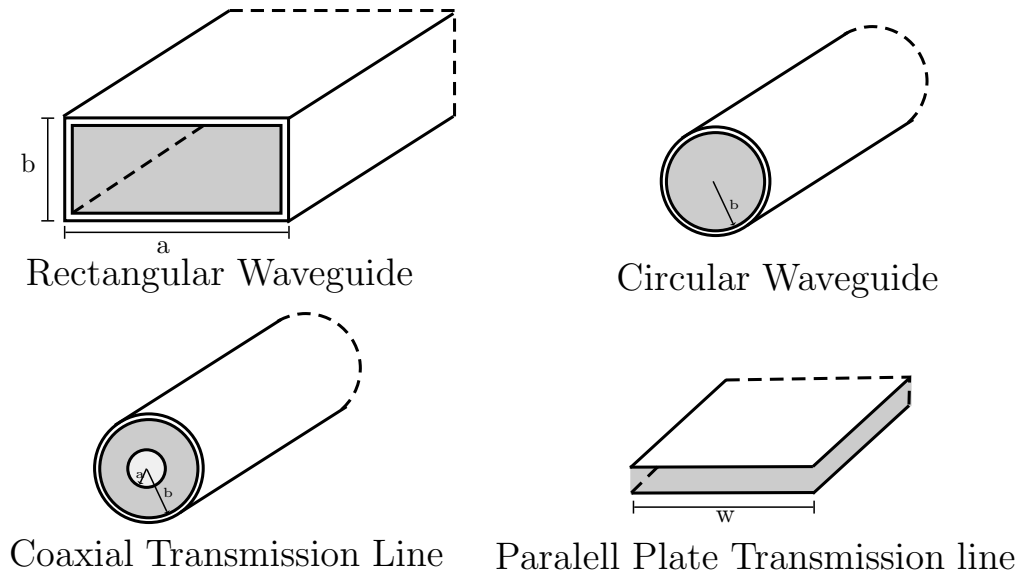


FIGURE 2.1: Types of Waveguides and Transmission Lines

$$\bar{E}(x, y, z) = [\hat{x}e_x(x, y) + \hat{y}e_y(x, y) + \hat{z}e_z(x, y)]e^{-j\beta z} \quad (2.1)$$

$$\bar{H}(x, y, z) = [\hat{x}h_x(x, y) + \hat{y}h_y(x, y) + \hat{z}h_z(x, y)]e^{-j\beta z} \quad (2.2)$$

Here β , the propagation constant, is a real number. $j\beta$ must be replaced with $\gamma = \alpha + j\beta$ if attenuation is also to be considered.

Then, if the dielectric in the waveguide has no charges or currents, we can write Maxwell's equations as

$$\nabla \times \bar{E} = -j\omega\mu\bar{H} \quad (2.3a)$$

$$\nabla \times \bar{H} = j\omega\epsilon\bar{E} \quad (2.3b)$$

Taking the curl of 2.3a gives

$$\nabla \times \nabla \times \bar{E} = -j\omega\mu\nabla \times \bar{H} = \omega^2\mu\epsilon\bar{E} \quad (2.4)$$

Using the vector identity $\nabla \times \nabla \times \bar{A} = \nabla(\nabla \cdot \bar{A}) - \nabla^2 \bar{A}$ and $\nabla \cdot \bar{E} = 0$ for a region with no sources ($\rho = 0$) we get

$$\nabla^2 \bar{E} + \omega^2 \mu \epsilon \bar{E} = 0 \quad (2.5)$$

Similarly, we can also take the curl of 2.3b to get

$$\nabla^2 \bar{H} + \omega^2 \mu \epsilon \bar{H} = 0 \quad (2.6)$$

For a z dependence of $e^{-j\beta z}$, E_z and H_z can be written as

$$\left(\frac{\partial^2}{\partial x^2} + \frac{\partial^2}{\partial y^2} + k^2 - \beta^2 \right) E_z = 0 \quad (2.7)$$

$$\left(\frac{\partial^2}{\partial x^2} + \frac{\partial^2}{\partial y^2} + k^2 - \beta^2 \right) H_z = 0 \quad (2.8)$$

since $\frac{\partial^2}{\partial z^2} (A e^{-j\beta z}) = -\beta A e^{-j\beta z}$. Let us define $k_c^2 = k^2 - \beta^2$ for convenience.

After writing down the 6 equations that arise from 2.3 and eliminating variables, we can write E_x, E_y, H_x, H_y in terms of E_z and H_z as follows

$$E_x = \frac{-j}{k_c^2} \left(\beta \frac{\partial E_z}{\partial x} + \omega \mu \frac{\partial H_z}{\partial y} \right) \quad (2.9a)$$

$$E_y = \frac{j}{k_c^2} \left(-\beta \frac{\partial E_z}{\partial y} + \omega \mu \frac{\partial H_z}{\partial x} \right) \quad (2.9b)$$

$$H_x = \frac{j}{k_c^2} \left(\omega \epsilon \frac{\partial E_z}{\partial y} - \beta \frac{\partial H_z}{\partial x} \right) \quad (2.9c)$$

$$H_y = \frac{-j}{k_c^2} \left(\omega \epsilon \frac{\partial E_z}{\partial x} + \beta \frac{\partial H_z}{\partial y} \right) \quad (2.9d)$$

where

$$k_c^2 = k^2 - \beta^2 \quad (2.10)$$

$$k = \omega \sqrt{\mu \epsilon} = 2\pi/\lambda \quad (2.11)$$

These equations (2.7, 2.8 and 2.9) can be used for any waveguide. There are three types of waves that are possible in waveguides: Transverse Electric and Magnetic mode (TEM), Transverse Electric mode (TE) and Transverse Magnetic mode (TM).

1. TEM modes

In this mode $E_z = H_z = 0$, meaning there are only transverse fields.

2. TE modes

In this mode $E_z = 0$, meaning there are only transverse electric fields.

3. TM modes

In this mode $H_z = 0$, meaning there are only transverse magnetic fields.

Rectangular Waveguide

Let us now concentrate on the fields in a rectangular waveguide. It can be shown that in the TEM mode, fields in the dielectric follow the same rules as electrostatics [16]. In a single conductor waveguide like the rectangular waveguide, the electrostatic potential is zero (or constant) which means that $E = 0$ and $H = 0$. This means we can only have TE and TM modes in the rectangular waveguide (or any single conductor waveguide).

1. TE modes

Equation 2.8 has been rewritten below with $k^2 - \beta^2$ replaced with k_c and divided by $e^{-j\beta z}$.

$$\left(\frac{\partial^2}{\partial x^2} + \frac{\partial^2}{\partial y^2} + k_c^2 \right) h_z = 0 \quad (2.12)$$

Here, $H_z(x, y, z) = h_z(x, y)e^{-j\beta z}$.

We can solve 2.12 using separation of variables. We assume

$$h_z(x, y) = F(x)G(y) \quad (2.13)$$

Substituting this into 2.12 gives

$$\frac{1}{F} \frac{d^2F}{dx^2} + \frac{1}{G} \frac{d^2G}{dy^2} + k_c^2 = 0 \quad (2.14)$$

Now, since each term is independent of each other, each term must be a constant. We define the first term to be k_x^2 and the second term to be k_y^2 to get

$$k_x^2 + k_y^2 + k_c^2 = 0 \quad (2.15)$$

Then we get 2 ordinary differential equations

$$\frac{d^2F}{dx^2} + k_x F = 0 \quad (2.16a)$$

$$\frac{d^2G}{dy^2} + k_y G = 0 \quad (2.16b)$$

The general solution to 2.16 is

$$F = A \cos(k_x x) + B \sin(k_x x) \quad (2.17a)$$

$$G = C \cos(k_y y) + D \sin(k_y y) \quad (2.17b)$$

Which gives

$$h_z = (A \cos(k_x x) + B \sin(k_x x))(C \cos(k_y y) + D \sin(k_y y)) \quad (2.18)$$

Since the boundary conditions we have are that the tangential electric field at the conductor is zero, i.e.

$$e_x(x, y) = 0 \quad \text{at } y = 0 \text{ and } y = b \quad (2.19a)$$

$$e_y(x, y) = 0 \quad \text{at } x = 0 \text{ and } x = a \quad (2.19b)$$

Substituting $E_z = 0$ in 2.9, we get

$$E_x = \frac{-j\omega\mu}{k_c^2} \frac{\partial H_z}{\partial y} \quad (2.20a)$$

$$E_y = \frac{-j\omega\mu}{k_c^2} \frac{\partial H_z}{\partial x} \quad (2.20b)$$

$$H_x = \frac{-j\beta}{k_c^2} \frac{\partial H_z}{\partial x} \quad (2.20c)$$

$$H_y = \frac{-j\beta}{k_c^2} \frac{\partial H_z}{\partial y} \quad (2.20d)$$

Now substituting $h_z(x, y)$ from 2.18 we get the following electric fields

$$e_x = \frac{-j\omega\mu}{k_c^2} k_y (A \cos(k_x x) + B \sin(k_x x)) (-C \sin(k_y y) + D \cos(k_y y)) \quad (2.21a)$$

$$e_y = \frac{j\omega\mu}{k_c^2} k_x (-A \sin(k_x x) + B \cos(k_x x)) (C \cos(k_y y) + D \sin(k_y y)) \quad (2.21b)$$

Now applying the boundary conditions,

from 2.19a we get $D = 0$ and $k_y = n\pi/b$ for $n = 0, 1, 2 \dots$,

and from 2.19b we get $B = 0$ and $k_x = m\pi/a$ for $m = 0, 1, 2 \dots$

From this we know the propagation constant is

$$\beta = \sqrt{k^2 - k_c^2} = \sqrt{k^2 - \left(\frac{m\pi}{a}\right)^2 - \left(\frac{n\pi}{b}\right)^2} \quad (2.22)$$

Since β is real, we now have a cut-off frequency for which $k^2 > k_c^2$. This means that if $a > b$, there will be a range of frequencies for which $TE_{mn} = TE_{10}$ will have propagation but TE_{01} will not.

The final solution for H_z is

$$H_z(x, y, z) = A_{mn} \cos\left(\frac{m\pi x}{a}\right) \cos\left(\frac{n\pi y}{b}\right) e^{-j\beta z} \quad (2.23)$$

where $A_{mn} = AC$.

Now we can find E_x, E_y, H_x and H_y using 2.20

$$E_x(x, y, z) = \frac{j\omega\mu n\pi}{k_c^2 b} A_{mn} \cos\left(\frac{m\pi x}{a}\right) \sin\left(\frac{n\pi y}{b}\right) e^{-j\beta z} \quad (2.24a)$$

$$E_y(x, y, z) = \frac{-j\omega\mu m\pi}{k_c^2 a} A_{mn} \sin\left(\frac{m\pi x}{a}\right) \cos\left(\frac{n\pi y}{b}\right) e^{-j\beta z} \quad (2.24b)$$

$$H_x(x, y, z) = \frac{j\beta m\pi}{k_c^2 a} A_{mn} \sin\left(\frac{m\pi x}{a}\right) \cos\left(\frac{n\pi y}{b}\right) e^{-j\beta z} \quad (2.24c)$$

$$H_y(x, y, z) = \frac{j\beta n\pi}{k_c^2 b} A_{mn} \cos\left(\frac{m\pi x}{a}\right) \sin\left(\frac{n\pi y}{b}\right) e^{-j\beta z} \quad (2.24d)$$

These equations are only for a wave propagating in one direction. The total electric field well have another term for the fields with a different constant. We can replace A_{mn} with A_{mn}^+ (for $+z$ direction propagation) and A_{mn}^- (for $-z$ direction propagation). Then the transverse fields for each mode (m, n) would take the form

$$\bar{E}_t(x, y, z) = [\hat{x}e_x(x, y) + \hat{y}e_y(x, y)](A^+ e^{-j\beta z} + A^- e^{+j\beta z}) \quad (2.25a)$$

$$\bar{H}_t(x, y, z) = [\hat{x}h_x(x, y) + \hat{y}h_y(x, y)](A^+ e^{-j\beta z} - A^- e^{+j\beta z}) \quad (2.25b)$$

The negative sign for A^- in the magnetic field is to ensure that the direction of propagation given by $\bar{E}_t \times \bar{H}_t$ is opposite.

2. TM modes

The TM modes can be derived in exactly the same way except that the boundary conditions will apply directly to E_z this time.

The fields for the TM modes are

$$E_z(x, y, z) = B_{mn} \sin\left(\frac{m\pi x}{a}\right) \sin\left(\frac{n\pi y}{b}\right) e^{-j\beta z} \quad (2.26a)$$

$$E_x(x, y, z) = \frac{-j\beta m\pi}{k_c^2 a} B_{mn} \cos\left(\frac{m\pi x}{a}\right) \sin\left(\frac{n\pi y}{b}\right) e^{-j\beta z} \quad (2.26b)$$

$$E_y(x, y, z) = \frac{-j\beta n\pi}{k_c^2 b} B_{mn} \sin\left(\frac{m\pi x}{a}\right) \cos\left(\frac{n\pi y}{b}\right) e^{-j\beta z} \quad (2.26c)$$

$$H_x(x, y, z) = \frac{j\omega\epsilon n\pi}{k_c^2 b} B_{mn} \sin\left(\frac{m\pi x}{a}\right) \cos\left(\frac{n\pi y}{b}\right) e^{-j\beta z} \quad (2.26d)$$

$$H_y(x, y, z) = \frac{-j\omega\epsilon m\pi}{k_c^2 a} B_{mn} \cos\left(\frac{m\pi x}{a}\right) \sin\left(\frac{n\pi y}{b}\right) e^{-j\beta z} \quad (2.26e)$$

Notice that if m or n is zero, then the fields all go to zero. So there is no TM_{10} or TM_{01} mode.

The propagation constant β is

$$\beta = \sqrt{k^2 - k_c^2} = \sqrt{k^2 - \left(\frac{m\pi}{a}\right)^2 - \left(\frac{n\pi}{b}\right)^2} \quad (2.27)$$

This means the cut-off frequencies are the same for the TE and TM modes.

Now we can see that there is a range of frequencies where only the TE_{10} mode will propagate. This feature of waveguides is used extensively to avoid complications of other modes interfering with the signal.

2.1.2 Rectangular Waveguide Resonators

Now that we know what modes and what frequencies can propagate in a rectangular waveguide, we can convert the waveguide into a resonator by walling the 2 infinitely open faces with conducting surfaces to make a cuboid filled with dielectric. This structure is often called a rectangular cavity.

We can use the equations we derived in the previous section for fields and the propagation constant to see what effects the new conducting walls will have.

We can start by writing down the transverse electric field ($E_t = \hat{x}E_x + \hat{y}E_y$)

$$\bar{E}_t = \bar{e}(x, y)(A^+e^{-j\beta z} + A^-e^{+j\beta z}) \quad (2.28)$$

where $\bar{e}(x, y)$ is the variation in the transverse fields.

$$\beta = \sqrt{k^2 - \left(\frac{m\pi}{a}\right)^2 - \left(\frac{n\pi}{b}\right)^2} \quad (2.29)$$

The new boundary conditions added now are that $E_t = 0$ at the 2 new walls, $z = 0$ and $z = d$.

For $z = 0$, 2.28 gives

$$A^+ = -A^- \quad (2.30)$$

For $z = d$, 2.28 gives

$$-\bar{e}(x, y)A^+2j \sin(\beta_{mn}d) = 0 \quad (2.31)$$

The solution to this equation (other than $A^+ = 0$) is

$$\beta_{mn} = \frac{l\pi}{d} \text{ where } l = 1, 2, 3 \dots \quad (2.32)$$

This means that, given a frequency, propagation (or in this case resonance) occurs only for particular lengths. $\beta^2 = k^2 - k_c^2$ can be rearranged to get

$$k_{mnl} = \sqrt{\left(\frac{m\pi}{a}\right)^2 + \left(\frac{n\pi}{b}\right)^2 + \left(\frac{l\pi}{d}\right)^2} \quad (2.33)$$

The resonant frequency is given by

$$f_{mnl} = \frac{ck_{mnl}}{2\pi\sqrt{\mu_r\epsilon_r}} = \frac{c}{2\pi\sqrt{\mu_r\epsilon_r}} \sqrt{\left(\frac{m\pi}{a}\right)^2 + \left(\frac{n\pi}{b}\right)^2 + \left(\frac{l\pi}{d}\right)^2} \quad (2.34)$$

Now let us restrict ourselves to the TE_{10l} mode of the resonator. Since $A^- = -A^+$, the fields for this mode are

$$E_y(x, y, z) = A^+ \sin\left(\frac{\pi x}{a}\right) (e^{-j\beta z} - e^{+j\beta z}) \quad (2.35a)$$

$$H_x(x, y, z) = \frac{-A^+}{Z_{TE}} \sin\left(\frac{\pi x}{a}\right) (e^{-j\beta z} + e^{+j\beta z}) \quad (2.35b)$$

$$H_z(x, y, z) = \frac{j\pi A^+}{k\eta a} \cos\left(\frac{\pi x}{a}\right) (e^{-j\beta z} - e^{+j\beta z}) \quad (2.35c)$$

where

$$A^+ = \frac{-j\omega\mu m\pi}{k_c^2 a}$$

$$Z_{TE} = \frac{\omega\mu}{\beta} \quad k = \omega\sqrt{\mu\epsilon}$$

$$k_c^2 = \sqrt{\frac{\pi}{a}} \quad \eta = \sqrt{\frac{\mu}{\epsilon}}$$

Using $-2jA^+ = E_0$, we can simplify the above equations to

$$E_y(x, y, z) = E_0 \sin\left(\frac{\pi x}{a}\right) \sin\left(\frac{l\pi z}{d}\right) \quad (2.37a)$$

$$H_x(x, y, z) = \frac{-jE_0}{Z_{TE}} \sin\left(\frac{\pi x}{a}\right) \cos\left(\frac{l\pi z}{d}\right) \quad (2.37b)$$

$$H_z(x, y, z) = \frac{j\pi E_0}{k\eta a} \cos\left(\frac{\pi x}{a}\right) \sin\left(\frac{l\pi z}{d}\right) \quad (2.37c)$$

We can now calculate the *quality factor* Q by calculating the energy stored and power lost in the resonator. The stored electric energy is, from [16]

$$W_e = \frac{\epsilon}{4} \int_V E_y E_y^* dv = \frac{\epsilon abd}{16} E_0^2 \quad (2.38)$$

and the stored magnetic energy is

$$\begin{aligned}
 W_m &= \frac{\mu}{4} \int_V (H_x H_x^* + H_z H_z^*) dv \\
 &= \frac{\mu abd}{16} E_0^2 \left(\frac{1}{Z_{TE}^2} + \frac{\pi^2}{k^2 \eta^2 a^2} \right) \\
 &= \frac{\mu abd}{16} E_0^2 \left(\frac{\beta^2 + (\pi/a)^2}{k^2 \eta^2} \right) \\
 &= \frac{\mu abd}{16} E_0^2 \left(\frac{1}{\eta^2} \right) \\
 &= \frac{\epsilon abd}{16} E_0^2
 \end{aligned} \tag{2.39}$$

Note that $W_e = W_m$ at resonance.

The power lost by the conducting walls is

$$P_c = \frac{R_s}{2} \int_{walls} |H_t|^2 ds \tag{2.40}$$

where $R_s = \sqrt{\omega \mu_0 / (2\sigma)}$ is the surface resistivity and H_t is the tangential magnetic field at the walls. This gives

$$P_c = \frac{R_s E_0^2 \lambda^2}{8\eta^2} \left(\frac{l^2 ab}{d^2} + \frac{bd}{a^2} + \frac{l^2 a}{2d} + \frac{d}{2a} \right) \tag{2.41}$$

The power dissipated from the lossy dielectric with $\epsilon = \epsilon' - j\epsilon''$ is

$$P_d = \frac{1}{2} \int_V \bar{J} \cdot \bar{E} = \frac{\omega \epsilon''}{2} \int_V |\bar{E}|^2 dv = \frac{abd\omega \epsilon'' |E_0|^2}{8} \tag{2.42}$$

The quality factor Q is defined as

$$\begin{aligned}
 Q &= \omega \frac{\text{average energy stored}}{\text{average power loss}} \\
 &= \omega \frac{W_e + W_m}{P_{loss}} \\
 &= \omega \frac{2W_e}{P_c + P_d}
 \end{aligned} \tag{2.43}$$

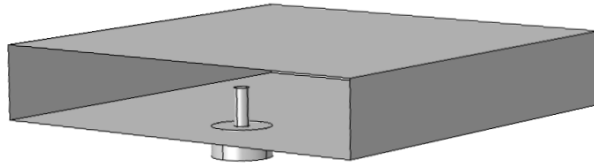


FIGURE 2.2: The probe is inserted up to a height h into the cavity. The other end of the probe is a coaxial cable whose outer terminal is connected to the cavity.

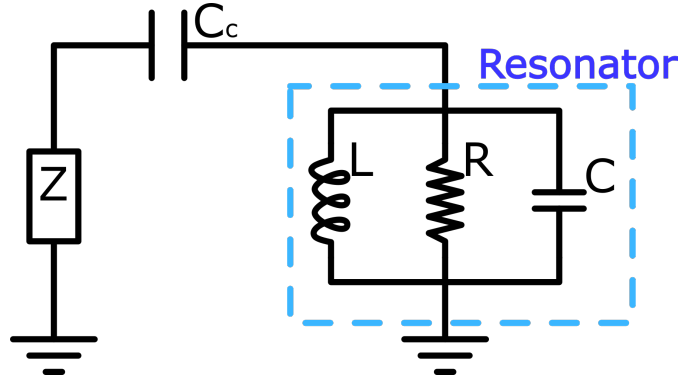


FIGURE 2.3: The equivalent circuit for the resonator is a parallel RLC circuit. The external losses are in the external impedance Z of the measurement device. The energy in the resonator leaks to the external circuit at a rate $\kappa_e \propto 1/C_c$. The internal losses are due to the resistance R . The rate of intrinsic energy loss in the resonator is $\kappa_i = \kappa - \kappa_e$ where κ is the FWHM of the S_{11} response of the resonator.

2.1.3 Coupling to an External Circuit

A resonator is useless if we cannot communicate with it in some way. There are many ways of interacting with a resonator. In the experiments to follow, the rectangular cavity resonator will be coupled to an external circuit through a probe of height h inserted at the $y = 0$ wall at $x = a/4$ and $z = 0$. A figure of the probe inserted in the rectangular cavity is shown in Fig.2.2.

The equivalent circuit, shown in Fig.2.3 for this setup would be a parallel RLC circuit capacitively coupled to the measurement device, which in this case is a VNA (Vector Network Analyzer).

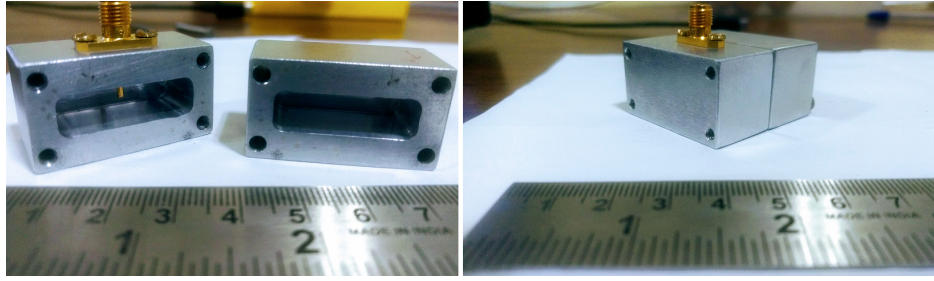


FIGURE 2.4: The Aluminium cavity used to make measurements. The dimensions of the hollow in the assembled cavity are $36 \times 27 \times 8\text{mm}$. The lengths of the connector pin referred to by Fig.2.7 includes the wall of the cavity.

2.2 Experiment

The rectangular cavity used for the experiment is made of aluminium and is shown in Fig.2.4.

The S_{11} parameter is the ratio of the voltage detected to voltage sent into the cavity. It is a complex number with information about the amplitude and phase. It is measured by sending a known signal of a particular frequency with a set amplitude and phase, and detecting the amplitude and phase of the reflected signal after passing through the cavity at the same frequency. A VNA is used to sweep the frequency of the input signal and record the amplitude and phase of the signal returned at the same frequency. The schematic of the circuit used to make measurements at $20mK$ is shown in Fig.2.5. The actual setup of the dilution refrigerator is shown in Fig.2.6.

The S_{11} response for a microwave resonator is given by [1]

$$S_{11}(\omega) = 1 - \frac{\kappa_e}{\kappa/2 + j(\omega - \omega_0)} \quad (2.44)$$

where

ω_0 is the resonant frequency of the cavity,

$\kappa = \Delta\omega$ is the FWHM of the resonance peak which represents total losses,

κ_e is the part of κ which represents the losses to the external circuit through the capacitor C_c .

The quality factor can be calculated using $Q = \omega_0/\text{FWHM}$. The internal, external

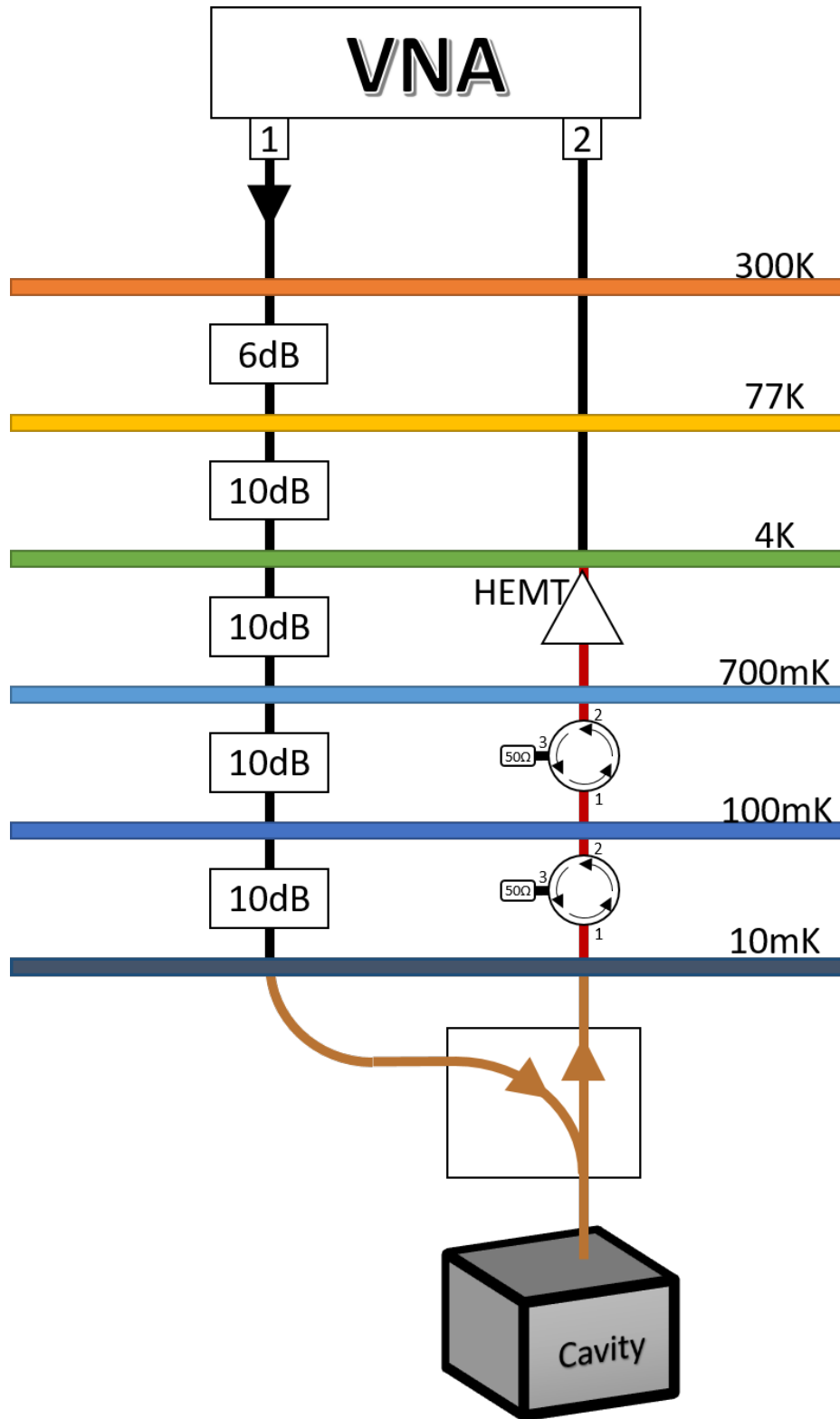


FIGURE 2.5: The measurement setup for $20mK$ measurements. The input signal is sent from port 1 of the VNA. There are attenuators of appropriate values in between the plates. At the base plate, the input goes into a directional coupler which adds another 20dB attenuation. The output from the cavity is directed towards a HEMT amplifier which is connected to port 2 of the VNA.



FIGURE 2.6: The Dilution Refrigerator.

and total quality factors can be calculated using

$$Q_{total} = \frac{\omega_0}{\kappa} \quad (2.45)$$

$$Q_{external} = \frac{\omega_0}{\kappa_e} \quad (2.46)$$

$$Q_{internal} = \left(\frac{1}{Q_{total}} - \frac{1}{Q_{external}} \right)^{-1} \quad (2.47)$$

$$(2.48)$$

The S_{11} response of the cavity is asymmetrical, as shown in Fig. ??, due to the finite cable length and finite isolation of the directional coupler.

- The effect of the finite cable length is an added frequency dependent phase factor $\exp(2j\omega l/v_p)$ where l is the cable length and $v_p = c/\sqrt{\epsilon_r}$ is the phase velocity. The '2' in the expression is because the cable length is traversed twice. This factor is multiplied to the original expression for S_{11} in 2.44.
- The effect of the finite isolation of the directional coupler is modelled by considering a part of the signal as a complex background ($\alpha_i e^{j\phi}$) and the rest of the signal $((1 - \alpha_i)S_{11})$ as the S_{11} response.

So the final function used to fit the data from Fig.2.5 and get the parameters ω_0, κ and κ is

$$S_{11}(\omega) = \alpha_i e^{j\phi} + (1 - \alpha_i) \left(1 - \frac{\kappa_e}{\kappa/2 + j(\omega - \omega_0)} \right) e^{2j\omega l/v_p} \quad (2.49)$$

The S_{11} measurement was performed for different pin lengths¹ inserted into the cavity at room temperature. The quality factors obtained from this measurement is shown in Fig.2.7. The coupling Quality Factor Q_c increases with decreasing pin length, while the internal Quality Factor remains the same.

The same measurement is made by using a constant pin length of 4.5mm, but this time at a temperature of 20mK. The internal quality factor is larger than the coupling quality factor at this temperature mainly because aluminium is superconducting below 1.1K. Fig.2.9 shows a plot of Q_i , Q_c and Q_t as a function of the average number of photons in the cavity. A sample plot of amplitude and phase

¹The lengths of the connector pin referred to here includes the wall of the cavity. So, the actual length of the connector pin that is in the cavity is 5 mm lesser than the given length.

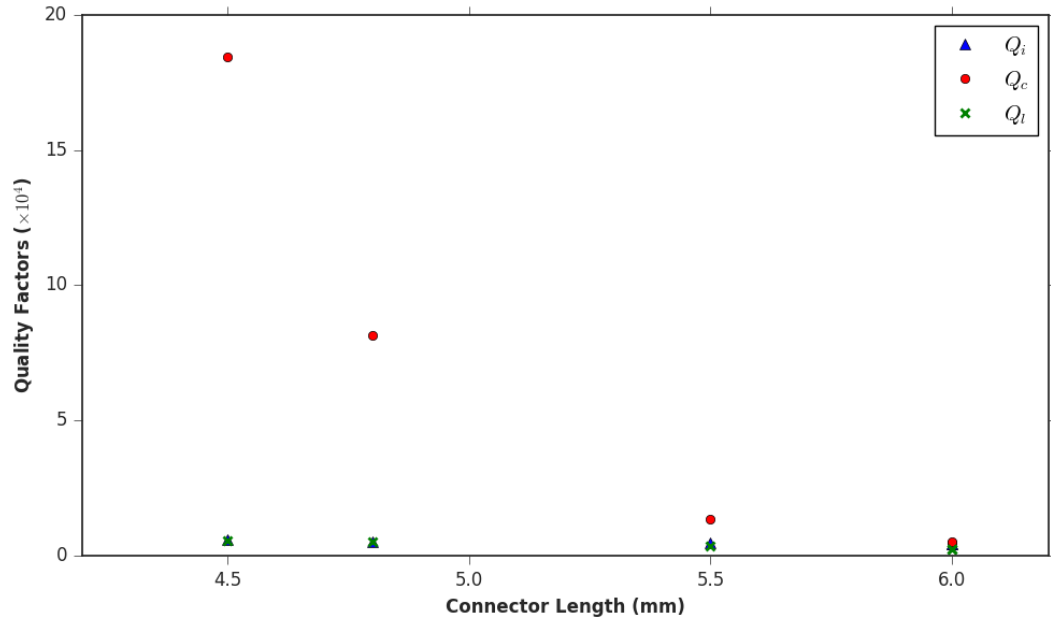


FIGURE 2.7: Quality factors for different pin lengths. Q_i is the internal Quality, Q_c is the external Quality, and Q_t is the total Quality. The coupling Quality Factor Q_c is increasing with decreasing pin lengths.

data for a power of -35dBm is shown in Fig.2.8. The coupling Quality Factor Q_c remains the same, suggesting that it does not depend on the number of photons in the cavity. The internal Quality Factor has an increasing trend. This can be explained using Two-Level Systems in the material which get saturated to their excited states at higher photon numbers[9].

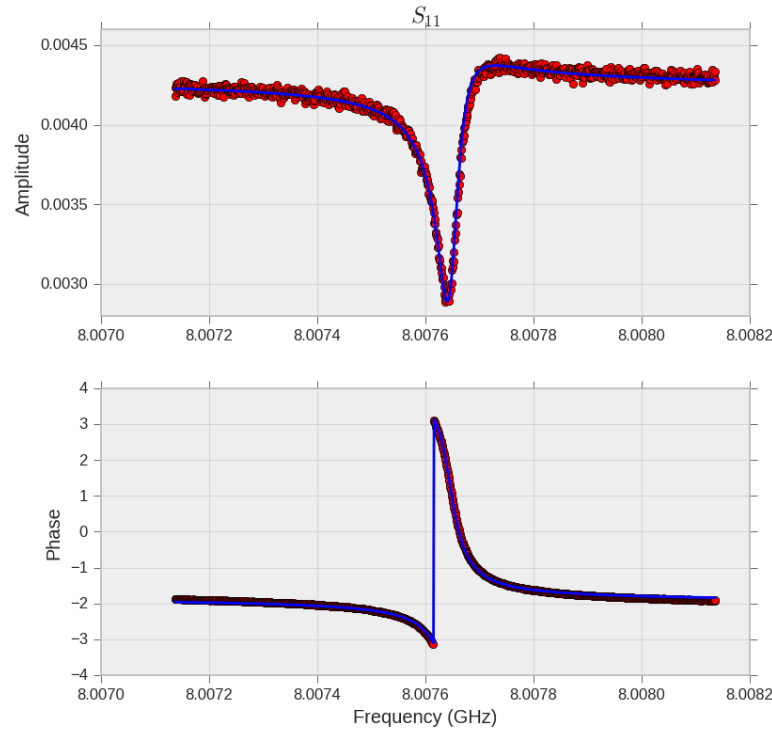


FIGURE 2.8: A sample of data and fit of S_{11} at 20mK for a power of -35dBm. The red dots are the data from the VNA, and the blue line is the fit.

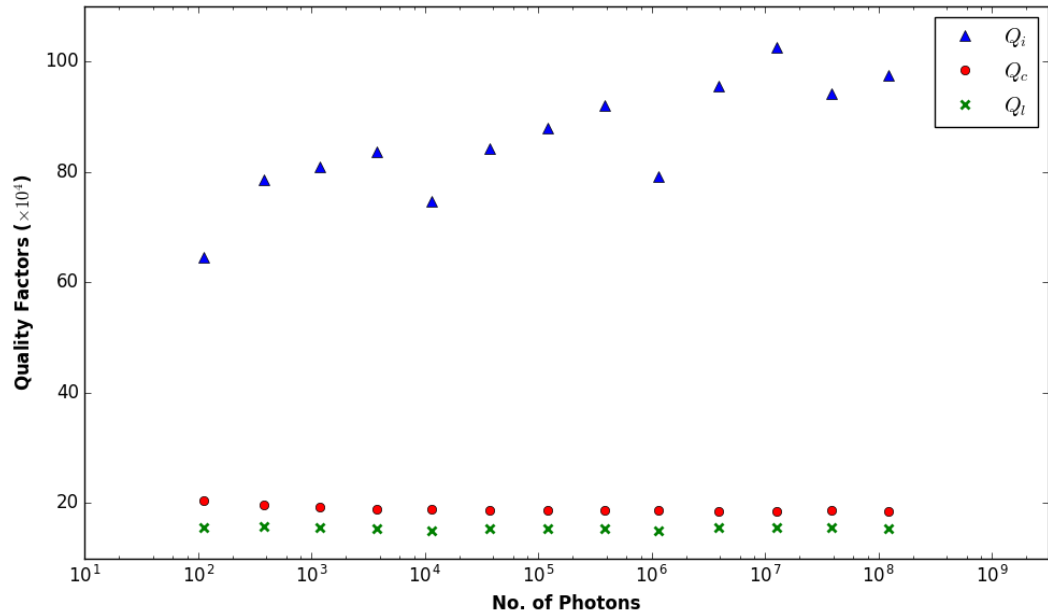


FIGURE 2.9: Quality factors for different powers at low temperature. Q_i is the internal Quality, Q_c is the external Quality, and Q_t is the total Quality.

Chapter 3

Superconducting Qubit Theory

3.1 Classical LC oscillator

The LC oscillator, shown in Fig.3.1, when treated classically has a charge q on the capacitor, and a flux ϕ in the inductor. The flux is related to the charge via the inductance as $\phi = L \frac{dq}{dt}$. The Hamiltonian for this circuit is

$$\mathcal{H} = \frac{q^2}{2C} + \frac{\phi^2}{2L} \quad (3.1)$$

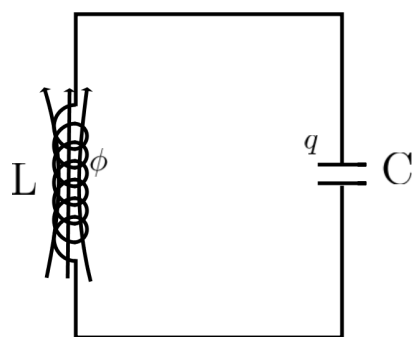


FIGURE 3.1: LC oscillator circuit

3.2 Quantum Electrical Circuits

3.2.1 Quantum LC oscillator

Observe that the 2 variables involved in the LC oscillator, q and $\phi = L \frac{dq}{dt}$, are similar in form to the position and momentum operators in quantum mechanics, \hat{x} and $\hat{p} = -j\hbar \frac{\partial}{\partial x}$. Even the Hamiltonian is of the same form.[7]

$$\hat{\mathcal{H}} = \frac{\hat{p}^2}{2m} + \frac{m\omega^2 \hat{x}^2}{2} \quad (3.2)$$

Because of this, we can treat this circuit like the simple harmonic oscillator and introduce the annihilation and creation operators to define \hat{q} , $\hat{\phi}$ and Hamiltonian operators as

$$\hat{\phi} = \frac{1}{j} \sqrt{\frac{\hbar}{2Z_0}} (a - a^\dagger) \quad (3.3a)$$

$$\hat{q} = \sqrt{\frac{\hbar Z_0}{2}} (a + a^\dagger) \quad (3.3b)$$

$$\hat{\mathcal{H}} = \frac{\hbar\omega_0}{2} (a^\dagger a + a a^\dagger) = \hbar\omega_0 \left(a^\dagger a + \frac{1}{2} \right) \quad (3.3c)$$

where

$$[\hat{\phi}, \hat{q}] = -j\hbar \quad \omega_0 = \frac{1}{\sqrt{LC}} \quad Z_0 = \sqrt{\frac{L}{C}}$$

ω_0 and C in the LC oscillator is analogous to ω and m in the harmonic oscillator.

We can write the wave-functions of the energy eigenstates of the LC oscillator as

$$\langle x | 0 \rangle = \psi_0 = \left(\frac{C\omega_0}{\pi\hbar} \right)^{\frac{1}{4}} e^{-\left(\frac{C\omega_0}{2\hbar}\right)x^2} \quad (3.4)$$

This solution can be obtained using $a |0\rangle = 0$

The rest of the eigenstates can be obtained by using the creation operator a^\dagger since

$$a^\dagger |n\rangle = \sqrt{n+1} |n+1\rangle \quad (3.5)$$

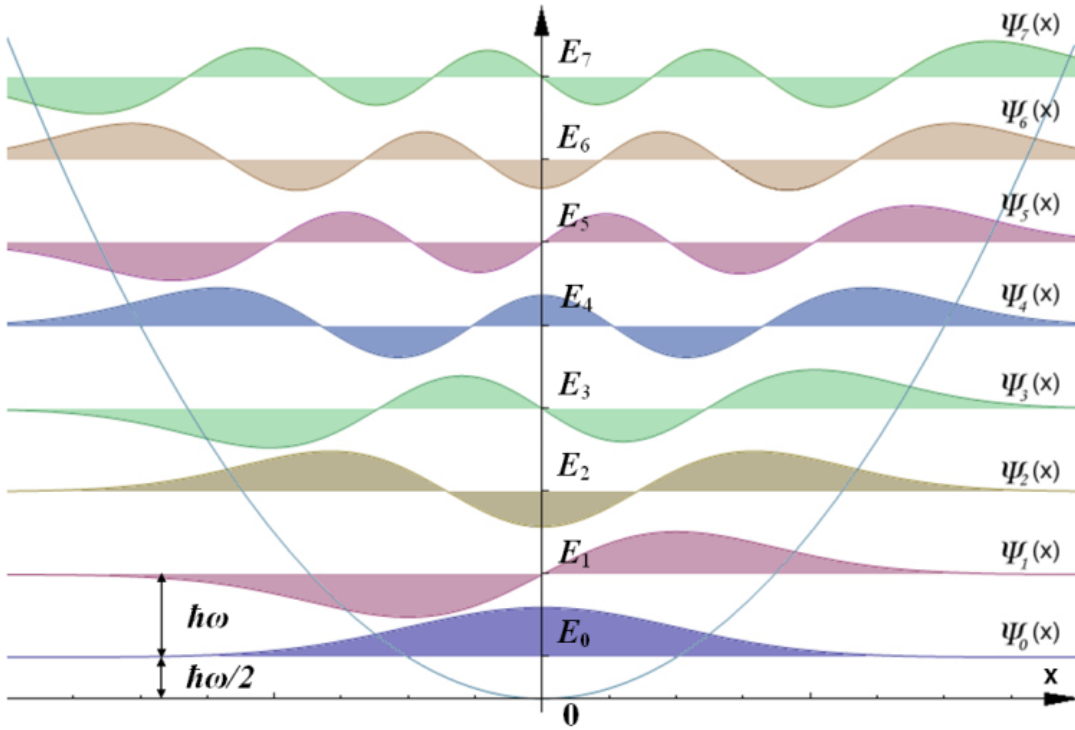


FIGURE 3.2: The harmonic oscillator potential showing the Energy Levels E_1, E_2, \dots along with the corresponding wavefunctions ψ_1, ψ_2, \dots . Replacing the position coordinate here with charge would give us the Energy levels for an LC oscillator. Taken from
 © User:Tomasz59 / Wikimedia Commons / CC-BY-SA-3.0

which gives

$$|n\rangle = \frac{(a^\dagger)^n}{\sqrt{n!}} |0\rangle \quad (3.6)$$

The energy corresponding to these states are

$$E_n = \left(n + \frac{1}{2} \right) \hbar\omega_0 \quad (3.7)$$

The general solution to the Schrödinger equation $\hat{\mathcal{H}} |\psi\rangle = E |\psi\rangle$ is

$$|\psi\rangle = \sum_n c_n |n\rangle \quad (3.8)$$

The first few energy levels along with the corresponding wavefunctions are shown in Fig.3.2.

Coherent states of a harmonic oscillator are defined as the eigenstates of the amplitude operator, or annihilation operator a , such that

$$a |\alpha\rangle = \alpha |\alpha\rangle \quad (3.9)$$

where $\alpha = |\alpha|e^{j\varphi}$ is a complex number and corresponds to the complex wave amplitude in classical optics. Thus coherent states are wave-like states of the electromagnetic oscillator is a complex number [11].

The coherent state $|\alpha\rangle$ can be represented in terms of the number states $|n\rangle$ as

$$|\alpha\rangle = \sum_{n=0}^{\infty} \frac{\alpha^n}{\sqrt{n!}} e^{-|\alpha|^2/2} |n\rangle \quad (3.10)$$

3.2.2 Nonlinear Harmonic Oscillator

Note that the energy levels in the Simple Harmonic Oscillator (SHO) or the LC oscillator are equispaced. This means that if we supply a photon of energy $\hbar\omega_0$ to the LC oscillator, we can change the state from any $|n\rangle$ to $|n+1\rangle$, and all photons emitted due to the transition from $|n\rangle$ to $|n-1\rangle$ will have the same energy.

A Nonlinear Harmonic Oscillator is one where the energy levels do not increase linearly. We can create a nonlinear oscillator by adding a perturbation to the Hamiltonian. The new Hamiltonian will be of the form

$$\hat{\mathcal{H}} = \frac{q^2}{2C} + \frac{\phi^2}{2L} + \mathcal{H}' \quad (3.11)$$

where H' is the perturbation term. The energy levels for this new Hamiltonian can be written in terms of the unperturbed Hamiltonian using perturbation theory as

$$E_n = E_n^{(0)} + \left\langle n^{(0)} \left| \mathcal{H}' \right| n^{(0)} \right\rangle + \sum_{k \neq n} \frac{\left| \left\langle k^{(0)} \left| \mathcal{H}' \right| n^{(0)} \right\rangle \right|^2}{E_n^{(0)} - E_k^{(0)}} + \dots \quad (3.12)$$

where,

E_n is the new energy for the n th eigenstate,

$E_n^{(0)}$ is the energy for the n th eigenstate of the unperturbed Hamiltonian,

$\langle n^{(0)} | \mathcal{H}' | n^{(0)} \rangle$ is the first order correction to the energy and

$\sum_{k \neq n} \frac{|\langle k^{(0)} | \mathcal{H}' | n^{(0)} \rangle|^2}{E_n^{(0)} - E_k^{(0)}}$ is the second order correction to the energy.

If the perturbation \mathcal{H}' is not a constant (i.e $\mathcal{H}'(n) \neq \mathcal{H}'(m)$ where $n \neq m$), then we can access only the ground state and the first excited state with one frequency of photons. This is because if the particle is in the first excited state, and another photon of the same energy ($E_{10} = E_1 - E_0$) is supplied to the system, it will not excite the particle further.

This means that we can selectively access only 2 states. If we can manipulate such a 2 level system and its interactions, we have a qubit!

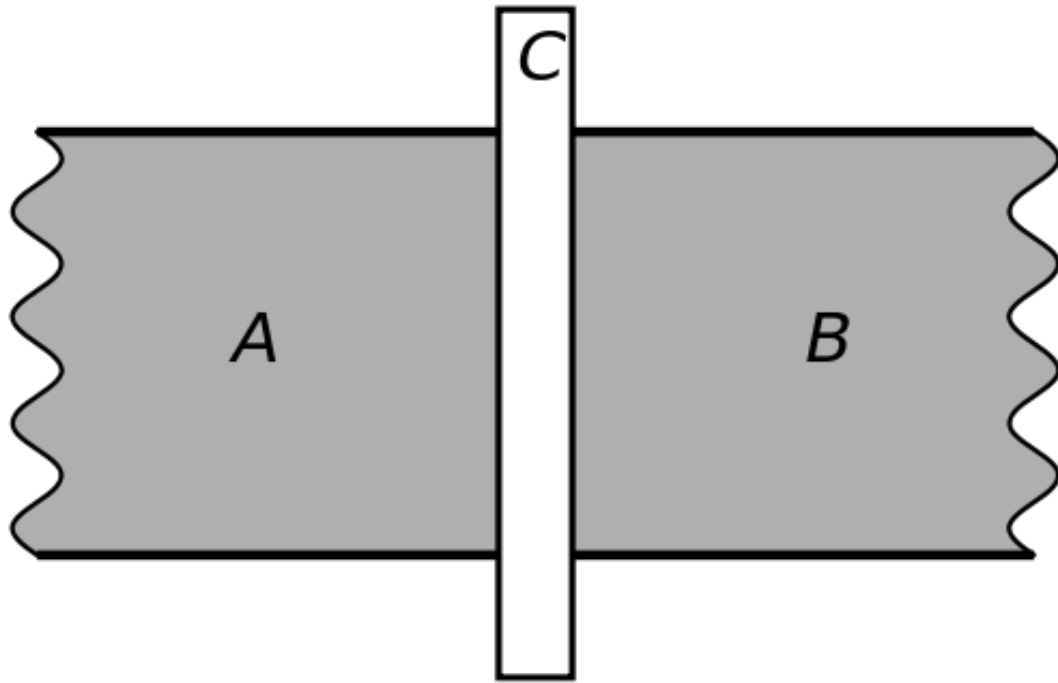


FIGURE 3.3: Simple geometric structure of a Josephson Junction with A and B being superconducting regions and C being the thin insulating layer.

3.3 The Josephson Junction

The Josephson Junction is the nonlinear element used in the described experiments due to its negligible dissipation rate which is essential for working in the quantum regime.

The Josephson Junction is made of 2 superconductors coupled by a weak link. In our case the junction is an S-I-S (Superconductor-Insulator-Superconductor) junction as shown in Fig.3.3.

Electrons in a normal metal behave like fermions. But at very low temperatures, they form cooper pairs that act like bosons. Nearly all the bosons will be at the lowest energy in exactly the same state [8]. This means that the superconductor will have a macroscopic wavefunction with a single homogeneous amplitude and phase.

In the Josephson Junction , there are two superconductors, and so we can define 2 amplitudes and 2 phases corresponding to each superconductor.

$$\psi_1 = \sqrt{\rho_1} e^{j\theta_1}$$

$$\psi_2 = \sqrt{\rho_2} e^{j\theta_2}$$

Then, the current and voltage characteristics are given by [12]

$$I_s = I_0 \sin \delta \quad (3.13)$$

$$V = \frac{\Phi_0}{2\pi} \dot{\delta} \quad (3.14)$$

where $\delta = \theta_2 - \theta_1$ is the superconducting phase difference¹ associated with the Josephson Junction , $\Phi_0 = h/2e$ is the flux quantum for a cooper pair and I_0 is the critical current of the junction.

We can view the Josephson Junction as a nonlinear inductor and find the inductance simply by using $V = L_J \frac{dI_s}{dt}$ which gives L_J , the Josephson Inductance to be

$$L_J = \frac{\Phi_0}{2\pi} \frac{1}{I_0 \cos \delta} \quad (3.15)$$

In addition to this we can represent a real Josephson Junction using the RCSJ model with a shunting capacitance (C) and resistance (R) along with the bare Josephson Junction [12]. Then the current through the circuit is

$$I = I_s + \frac{V}{R} + C \frac{dV}{dt} \quad (3.16)$$

by using 3.13 and 3.14 we get

$$C \left(\frac{\hbar}{2e} \right)^2 \frac{d^2\delta}{dt^2} + \frac{1}{R} \left(\frac{\hbar}{2e} \right)^2 \frac{d\delta}{dt} + \frac{\hbar}{2e} (I_0 \sin \delta - I) = 0 \quad (3.17)$$

We can see that this is the equation of motion of a particle moving along the δ coordinate with

an acceleration $\frac{d^2\delta}{dt^2}$,

¹This phase difference δ is the generalized phase difference $\delta = \Delta\theta - \frac{2\pi}{\Phi_0} \int A \cdot dl$

drag force proportional to velocity $\frac{d\delta}{dt}$ and
force due to the gradient of the potential energy as the last term.

This leads to the "particle mass" given by

$$M = C \left(\frac{\hbar}{2e} \right)^2 \quad \text{"particle mass"} \quad (3.18)$$

$$U(I, \delta) = -E_J \cos \delta - \left(\frac{\hbar}{2e} \right) I \delta \quad \text{potential energy} \quad (3.19)$$

where E_J , the Josephson Energy is given by

$$E_J = \frac{\hbar}{2e} I_0 = \frac{\Phi_0}{2\pi} I_0 \quad (3.20)$$

The current I is usually so small that we can ignore that term making the potential energy

$$U = -E_J \cos \delta \quad (3.21)$$

The electrical energy stored in the capacitance is analogous to kinetic energy and can be calculated as

$$E_{kin} = \frac{1}{2} M v^2 = \frac{1}{2} C \left(\frac{\hbar}{2e} \right)^2 \left(\frac{d\delta}{dt} \right)^2 \quad (3.22)$$

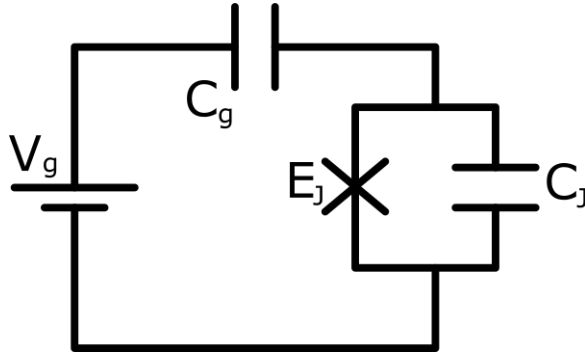


FIGURE 3.4: The Cooper Pair Box circuit with the Josephson Junction represented as a bare Josephson Junction with Josephson Energy E_J and a capacitance C_j .

3.4 The Cooper Pair Box

The Cooper Pair Box circuit is shown in Fig.3.4. It consists of a superconducting island capacitively coupled (with capacitance C_g) to a voltage source (V_g) connected to ground, and a Josephson Junction connected to the ground. The Josephson Junction can be represented by a capacitance (C_j) and the bare Josephson Junction (represented by E_J) as shown in the figure.

The electrical energy of this circuit is the energy stored in the 2 capacitors, C_g and C_j . If the total charge of the superconducting island is $-n|e|$, then the electrical energy (\mathcal{H}_{el}) is given by [19]

$$\hat{\mathcal{H}}_{el} = 4E_C(\hat{n} - n_g)^2 \quad (3.23)$$

where $\hat{n}|n\rangle = n|n\rangle$, $|n\rangle$ is the charge state with n cooper pairs.

$E_C = e^2/2C_\Sigma = e^2/2(C_j + C_g)$ is the energy required to add one electron to the island and $n_g = C_g V_g / e$.

The energy levels are shown in Fig.3.5 for $E_J = 0$. The Josephson Junction would allow charge to tunnel through at $n_g = 0.5, -0.5, 1.5, -1.5 \dots$ in order to maintain the lowest energy.

However, to calculate the complete Hamiltonian, we must also take into account the energy of the bare Josephson Junction (H_J) which is given by.

$$\hat{\mathcal{H}}_J = -E_J \cos \hat{\delta} \quad (3.24)$$

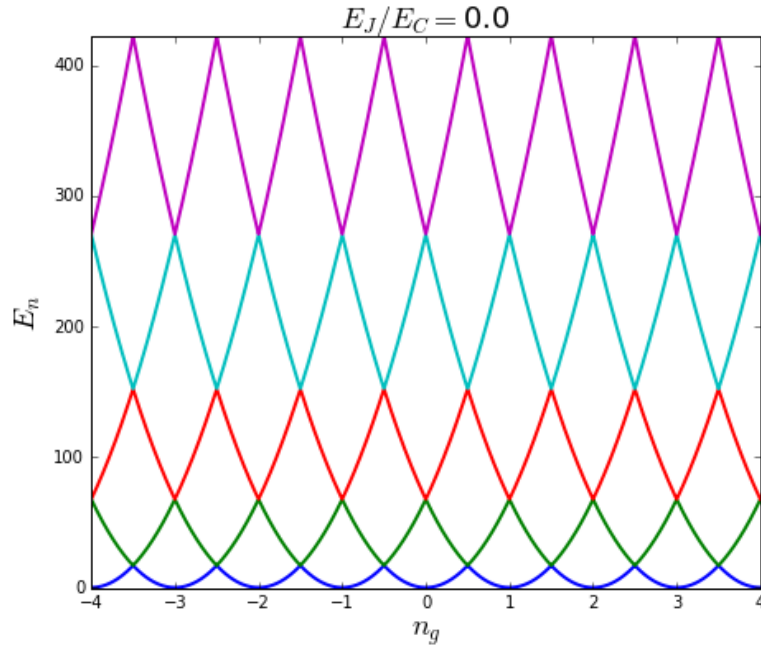


FIGURE 3.5: Energy levels for $E_J = 0$ or no tunneling. This figure was generated using [13].

This is the tunnelling energy in the phase basis. To find the expression in the charge basis, we start with the commutation relation between charge and phase (See Appendix 1-A-2 from [6]).

$$[\hat{n}, \hat{\delta}] = -j \quad (3.25)$$

Using 3.25 and the commutator identity 3.26, we get

$$[\hat{n}, \hat{\delta}^m] = \hat{\delta}^{m-1} [\hat{n}, \hat{\delta}] + \hat{\delta} [\hat{n}, \hat{\delta}^{m-1}] \quad (3.26)$$

$$(3.27)$$

we can recursively use this relation to get

$$[\hat{n}, \hat{\delta}^m] = -jm(\hat{\delta})^{m-1} \quad (3.28)$$

$$\hat{n}\hat{\delta}^m = -jm\hat{\delta}^{m-1} + \hat{\delta}^m\hat{n} \quad (3.29)$$

The operator $\hat{n}e^{jp\hat{\delta}}$, where $p \in Z$, after expansion is

$$\begin{aligned}\hat{n}e^{jp\hat{\delta}} &= \hat{n} \sum_{m=0}^{\infty} \frac{(jp\hat{\delta})^m}{m!} = \sum_{m=0}^{\infty} \frac{(jp)^m \hat{n} \hat{\delta}^m}{m!} \\ &= \sum_{m=0}^{\infty} \frac{(jp)^m \hat{n} (\hat{\delta})^m}{m!} \\ &= \sum_{m=0}^{\infty} \frac{(jp)^m (-jm\hat{\delta}^{m-1} + \hat{\delta}^m \hat{n})}{m!} \quad (3.30)\end{aligned}$$

$$\begin{aligned}&= \sum_{m=0}^{\infty} \frac{(jp)^m (-jm\hat{\delta}^{m-1})}{m!} + \sum_{m=0}^{\infty} \frac{(jp\hat{\delta})^m \hat{n}}{m!} \\ &= p \sum_{m=1}^{\infty} \frac{(jp\hat{\delta})^{m-1}}{(m-1)!} + \sum_{m=0}^{\infty} \frac{(jp\hat{\delta})^m \hat{n}}{m!}\end{aligned}$$

$$\hat{n}e^{jp\hat{\delta}} = pe^{jp\hat{\delta}} + e^{jp\hat{\delta}} \hat{n} \quad (3.31)$$

Using this operator on the charge state $|n\rangle$ gives

$$\hat{n}\{e^{jp\hat{\delta}}|n\rangle\} = pe^{jp\hat{\delta}}|n\rangle + e^{jp\hat{\delta}}\hat{n}|n\rangle \quad (3.32)$$

$$= (n+p)\{e^{jp\hat{\delta}}|n\rangle\} \quad (3.33)$$

$$\implies e^{jp\hat{\delta}}|n\rangle = |n+p\rangle \quad (3.34)$$

So, we can see that

$$e^{ip\hat{\delta}} = \sum_{m=-\infty}^{\infty} |m+p\rangle \langle m| \quad (3.35)$$

$$\begin{aligned}\cos \hat{\delta} &= \frac{1}{2} (e^{i\hat{\delta}} + e^{-i\hat{\delta}}) = \frac{1}{2} \left(\sum_{m=-\infty}^{\infty} |m+1\rangle \langle m| + \sum_{m=-\infty}^{\infty} |m-1\rangle \langle m| \right) \\ &= \frac{1}{2} \sum_{n=-\infty}^{+\infty} |n\rangle \langle n+1| + |n+1\rangle \langle n| \quad (3.36)\end{aligned}$$

$$\hat{\mathcal{H}}_J = -\frac{E_J}{2} \left(\sum_{n=-\infty}^{+\infty} |n\rangle \langle n+1| + |n+1\rangle \langle n| \right) \quad (3.37)$$

So the complete Hamiltonian in the charge basis is the sum of these

$$\hat{\mathcal{H}} = \sum_{n=-\infty}^{+\infty} \left(4E_C(\hat{n} - n_g)^2 |n\rangle \langle n| - \frac{E_J}{2} |n\rangle \langle n+1| + |n+1\rangle \langle n| \right) \quad (3.38)$$

In the phase basis we can replace \hat{n} with $-i\frac{\partial}{\partial\delta}$ to get

$$\hat{\mathcal{H}} = 4E_C \left(-i\frac{\partial}{\partial\delta} - n_g \right)^2 - E_J \cos \delta \quad (3.39)$$

The energy eigenstates $|k\rangle$ are given by the schrödinger equation

$$\hat{\mathcal{H}}(n_g) |k\rangle = E_k(n_g) |k\rangle \quad (3.40)$$

These eigenenergies can be solved analytically in the phase basis in terms of Mathieu functions. The eigenenergies are given by

$$E_k(n_g) = E_C a_{2[n_g+k(m,n_g)]}(-E_J/2E_C) \quad (3.41)$$

where $a_\nu(q)$ denotes Mathieu's characteristic value, and $k(m, n_g)$ is a function appropriately sorting the eigenvalues [14].

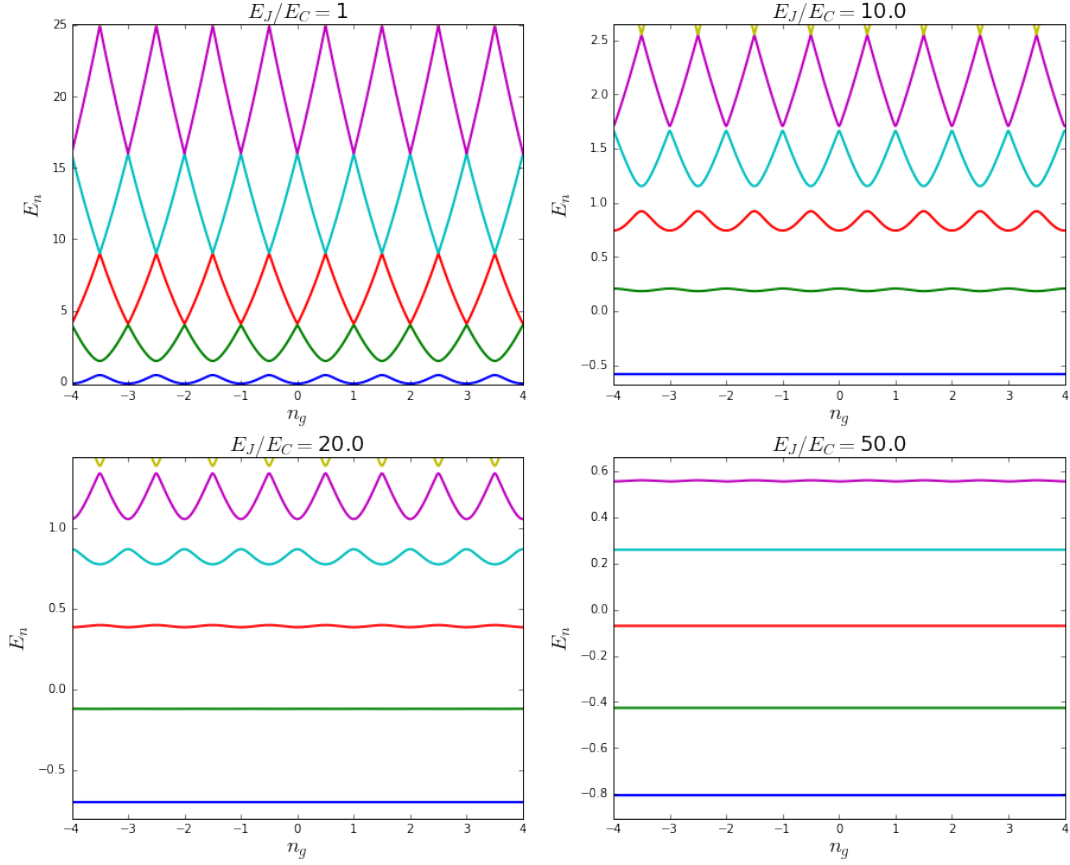


FIGURE 3.6: Energy levels for different E_J/E_C values. Charge noise goes to zero as E_J/E_C increases. Anharmonicity is also low but non-zero. This figure was generated using [13].

3.5 The 3D Superconducting Transmon

A Transmon is basically a Cooper Pair Box in which the Josephson Junction is shunted with a large capacitance in order to decrease E_C and so increase E_J/E_C .

The energy levels (E_k) plotted against gate charge (n_g) for different E_J/E_C values are shown in Fig.3.6.

As we can see the charge noise is very low for the case of high E_J/E_C . Also, anharmonicity, which is defined as $\alpha_h = E_{21} - E_{10}$, is reduced but not zero. In-fact, charge noise reduces exponentially while anharmonicity reduces only algebraically as E_J/E_C is increased. This is the basis on which the transmon qubit is realised.

The Hamiltonian can also be solved using perturbation theory in the limit $E_J/E_C \gg 1$ by expanding the cosine in the tunnelling energy up to fourth order and treating the fourth order term as a perturbation. There is no dependence on n_g because the

system is charge insensitive at high E_J/E_C . The energy levels are [14]

$$E_k \approx -E_J + \sqrt{8E_C E_J} \left(k + \frac{1}{2} \right) - \frac{E_C}{12} (6k^2 + 6k + 3) \quad (3.42)$$

From 3.42 we can see that the qubit transition frequency (ω_{10}) is

$$\omega_{10} = \frac{E_1 - E_0}{\hbar} = \frac{\sqrt{8E_J E_C} - E_C}{\hbar} \quad (3.43)$$

and the anharmonicity

$$\alpha_h = (E_2 - E_1) - (E_1 - E_0) = -E_C \quad (3.44)$$

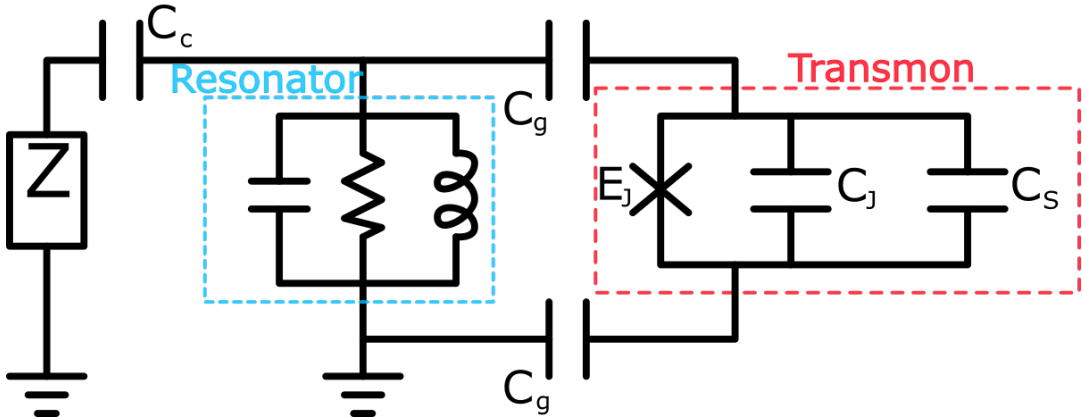


FIGURE 3.7: Transmon coupled to the resonator coupled to the measurement device.

3.6 Coupling the Transmon to a Resonator

For qubit readout and control, we will couple the qubit to a microwave cavity resonator (A rectangular waveguide resonator in this case). The lumped element circuit model of the qubit and cavity resonator is shown in Fig.3.7.

We can approximate the transmon as a 2 level system with a ground state $|g\rangle$ and excited state $|e\rangle$ for large anharmonicity. In this approximation, the Hamiltonian of the system is discussed below [18, 19].

- The Hamiltonian of the transmon can be expressed as the following if we choose the coordinate system appropriately and the zero energy as the mean energy of the transmon

$$\hat{\mathcal{H}}_{qubit} = -\frac{\hbar\omega_q}{2}\sigma_z \quad (3.45)$$

- The Hamiltonian of the resonator is the same as the one for an LC oscillator

3.3c

$$\hat{\mathcal{H}}_{cavity} = \hbar\omega_r a^\dagger a \quad (3.46)$$

The ground state energy of $\hbar\omega_r/2$ has not been shown as it does not have any significance in qubit dynamics.

- The interaction hamiltonian is given by

$$\hat{\mathcal{H}}_{int} = \hbar g(a^\dagger \sigma_- + a \sigma_+) \quad (3.47)$$

where g is the coupling constant, proportional to the amplitude of the signal. The rotating wave approximation is made here, ignoring terms with $a^\dagger \sigma_+$ and $a \sigma_-$.

This gives us the Jaynes-Cummings Hamiltonian

$$\hat{\mathcal{H}} = \hbar \omega_r a^\dagger a - \frac{\hbar \omega_q}{2} \sigma_z + \hbar g(a^\dagger \sigma_- + a \sigma_+) \quad (3.48)$$

The eigenstates for the coupled system are

$$|n, +\rangle = \cos \frac{\theta_n}{2} |e\rangle |n\rangle + \sin \frac{\theta_n}{2} |g\rangle |n+1\rangle \quad (3.49a)$$

$$|n, -\rangle = -\sin \frac{\theta_n}{2} |e\rangle |n\rangle + \cos \frac{\theta_n}{2} |g\rangle |n+1\rangle \quad (3.49b)$$

with eigenenergies

$$E_{n\pm} = \hbar \omega_r n \pm \frac{\sqrt{\hbar^2 \Delta^2 + 4g^2(n+1)}}{2} \quad (3.50)$$

where $\Delta = \omega_r - \omega_q$ and

$$\theta_n = \tan^{-1} \left(\frac{2g\sqrt{n+1}}{\hbar\Delta} \right) \quad (3.51)$$

3.7 The Bloch Sphere

A general pure state for a two level system can be represented as

$$|\psi\rangle = c_0 |0\rangle + c_1 |1\rangle \quad (3.52)$$

where $|0\rangle$ and $|1\rangle$ form an orthonormal basis. $c_0 = |c_0|e^{j\phi_1}$ and $c_1 = |c_1|e^{j\phi_2}$ are complex numbers with a constraint that $|c_0|^2 + |c_1|^2 = 1$ due to normalization. Since one can only measure the phase difference $\phi = \phi_2 - \phi_1$, the state can be represented as

$$|\psi\rangle = \cos \frac{\theta}{2} |0\rangle + e^{j\phi} \sin \frac{\theta}{2} |1\rangle \quad (3.53)$$

with no loss of generality where $\theta = 2 \cos^{-1} |c_0| = 2 \sin^{-1} |c_1|$.

This state can be represented on a sphere with spherical coordinates on the surface with radius $r = 1$. The $|0\rangle, |1\rangle$ and an arbitrary state is shown in the Bloch Sphere in Fig.3.8.

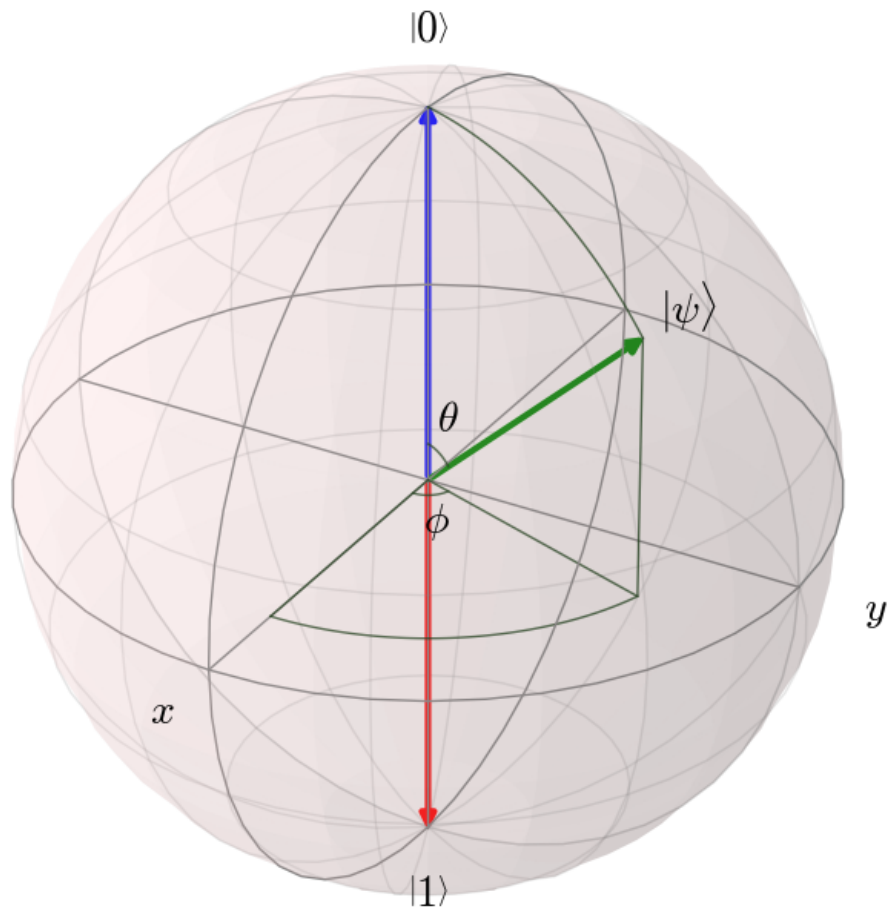


FIGURE 3.8: Representation of states on a Bloch Sphere. The blue arrow represents the ground state $|g\rangle$, the red arrow represents the excited state $|e\rangle$, and the green arrow represents an arbitrary state $|\psi\rangle = \cos(\theta/2) |g\rangle + e^{j\phi} \sin(\theta/2) |e\rangle$.

This figure was generated using [13].

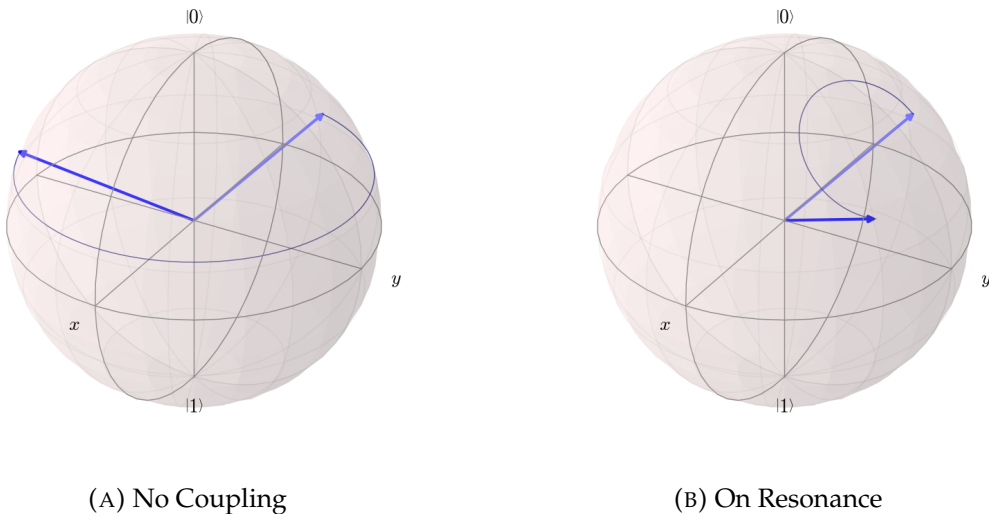


FIGURE 3.9: Evolution of an arbitrary state on the Bloch sphere. The light blue arrow represents the initial state and the dark blue arrow represents the final state. This figure was generated using [13].

3.8 Dynamics of the Jaynes-Cummings system

Let us consider the dynamics of the system in three different cases that are relevant to qubit manipulation and readout.

- Zero Coupling ($g = 0$)

If there is no coupling (no photons in the cavity), then the qubit follows the free Hamiltonian given by 3.45. The energy eigenstates of this system are $|g\rangle$ and $|e\rangle$ with energies $-\hbar\omega_q/2$ and $\hbar\omega_q/2$ respectively. In this basis, the Hamiltonian of the qubit can be expressed as

$$\hat{\mathcal{H}}_{gubit} = -\hbar\omega_g/2 |e\rangle\langle e| + \hbar\omega_g/2 |g\rangle\langle g| \quad (3.54)$$

Applying the unitary operator $e^{i\hat{H}t/\hbar}$ to an initial superposition state $|\psi(0)\rangle = c_0|e\rangle + c_1|g\rangle$ gives the state at a time t

$$\begin{aligned} |\psi(t)\rangle &= e^{i\hat{\mathcal{H}}t/\hbar} |\psi(0)\rangle \\ &= e^{-i\omega_q t/2} (c_0 |e\rangle + e^{i\omega_q t} c_1 |g\rangle) \end{aligned} \quad (3.55)$$

We can see that if the qubit starts in an eigenstate, it remains in the same state (only a phase factor is added), but if it starts in a superposition, its phase

oscillates as a function of time with a frequency equal to the qubit frequency. On the bloch sphere this can be represented as a precession about the z -axis as shown in Fig.3.9a.

We can consider the dynamics of the coupled system in a similar way, once we change the basis to the new energy eigenstates in 3.49.

- **On Resonance ($\Delta \ll g$)**

If the drive signal or photons are at the same frequency as the qubit, then $\Delta = 0$, which implies $\theta_n = \pi/2$. Then the eigenstates are

$$|n, +\rangle = \frac{1}{\sqrt{2}} |e\rangle |n\rangle + \frac{1}{\sqrt{2}} |g\rangle |n+1\rangle \quad (3.56a)$$

$$|n, -\rangle = -\frac{1}{\sqrt{2}} |e\rangle |n\rangle + \frac{1}{\sqrt{2}} |g\rangle |n+1\rangle \quad (3.56b)$$

With the new eigenstates, the qubit will oscillate about the x -axis as shown in Fig.3.9b. This means that if the initial state of the qubit is $|g\rangle$, it will oscillate to $|e\rangle$ in time $t = \pi g \sqrt{n+1}$. A pulsed signal which causes this transition² is called a π -pulse. The excitation number of the cavity will also oscillate from $|n+1\rangle$ to $|n\rangle$ with the same frequency.

It is worth noting that if the resonant frequency of the cavity is far from that of the qubit, and if the drive signal is of qubit frequency, then the qubit will still oscillate because it takes finite time for the photons to decay in the cavity.

- **Low Power Dispersive limit ($\Delta \gg g$)**

In the low power dispersive limit³, the number of photons in the cavity is low ($\approx 1-100$). We can rewrite the Hamiltonian by considering g/Δ as a perturbation since $\Delta \gg g$ [19] to get

$$\hat{\mathcal{H}} = \hbar \left(\omega_r + \frac{g^2}{\Delta} \sigma_z \right) a^\dagger a + \frac{\hbar}{2} \left(\omega_q + \frac{g^2}{\Delta} \right) \sigma_z \quad (3.57)$$

We can see from this Hamiltonian that dispersive coupling causes a shift of $\pm g^2/\Delta$ in the resonance frequency of the cavity depending on the qubit state.

²This signal refers to any signal which is resonant with the qubit and causes a rotation of π radians about the x -axis on the Bloch Sphere.

³For the high power limit see [3]. The specific case of the transmon in the high power limit is discussed in [5].

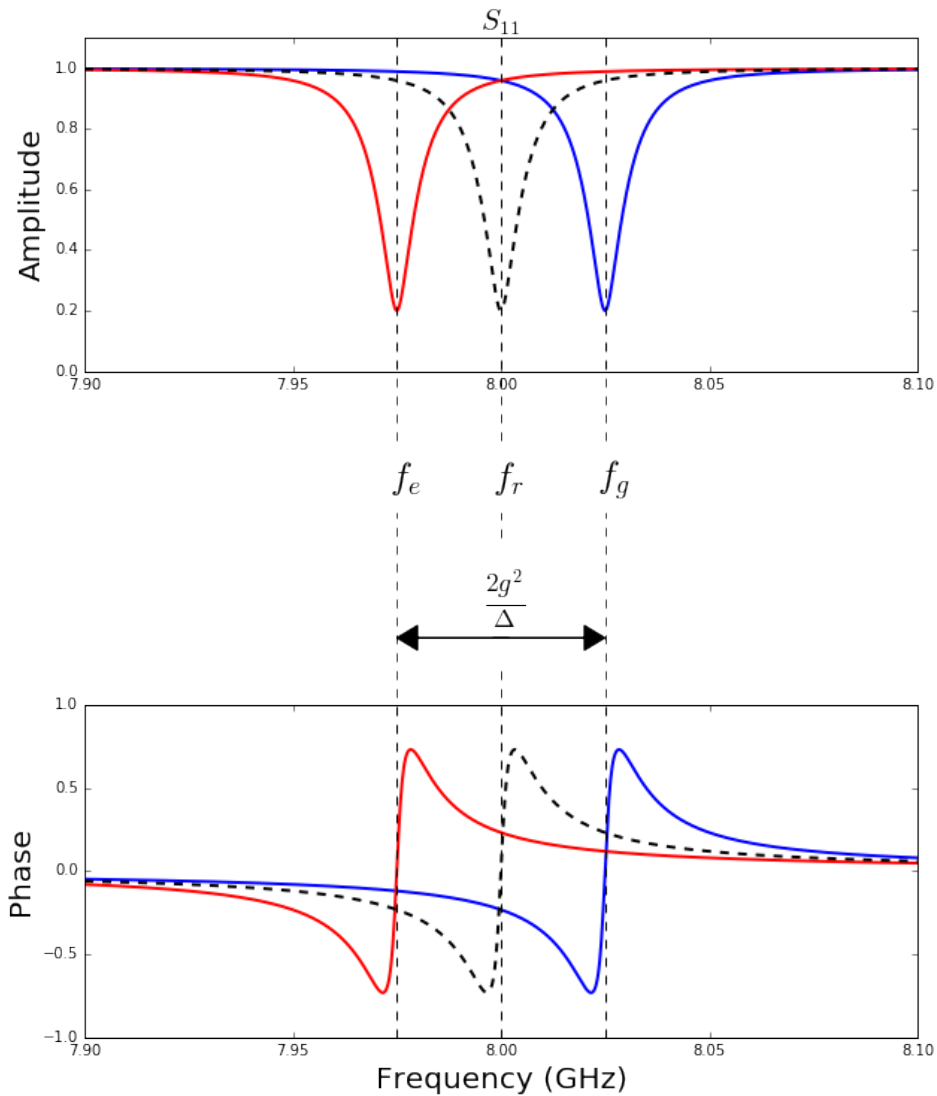


FIGURE 3.10: Amplitude and Phase of S_{11} for bare resonator (thick black dashed lines), resonator with qubit in ground state (thick blue line), and resonator with qubit in excited state (thick red line). The dispersive shift is $2g^2/\Delta$.

We can see the different S_{11} parameter responses for the ground and excited states of the qubit in Fig.3.10. This shift is crucial to measuring the state of the qubit. We can also rearrange the equation as follows

$$\hat{\mathcal{H}} = \hbar\omega_r a^\dagger a + \frac{\hbar}{2} \left(\omega_q + \frac{g^2}{\Delta} a^\dagger a + \frac{g^2}{\Delta} \right) \sigma_z \quad (3.58)$$

to see that the frequency of the qubit now has an added Lamb and ac-Stark shift of g^2/Δ and $g^2 n/\Delta$ respectively [4].

The Hamiltonian in 3.57 can be written as

$$\hat{\mathcal{H}} = \hat{\mathcal{H}}_0 + \hat{\mathcal{H}}_{int} \quad (3.59)$$

where

$$\hat{\mathcal{H}}_0 = \hbar\omega_r a^\dagger a + \frac{\hbar\omega_q}{2} \sigma_z \quad (3.60)$$

is the uncoupled Hamiltonian of the qubit and cavity and

$$\hat{\mathcal{H}}_{int} = \frac{\hbar g^2 \sigma_z}{\Delta} \left(a^\dagger a + \frac{1}{2} \right) \quad (3.61)$$

is the interaction Hamiltonian.

The unitary time evolution operator given by $\hat{U}(t) = e^{-j\hat{\mathcal{H}}t/\hbar}$ is

$$\begin{aligned} \hat{U}(t) = \exp \left(-j\hat{\mathcal{H}}_0 t / \hbar \right) & \left[\exp \left(-j \frac{g^2 t}{\Delta} \left(\hat{n} + \frac{1}{2} \right) \right) |g\rangle \langle g| \right. \\ & \left. + \exp \left(j \frac{g^2 t}{\Delta} \left(\hat{n} + \frac{1}{2} \right) \right) |e\rangle \langle e| \right] \end{aligned} \quad (3.62)$$

If the initial state is such that the cavity is in a coherent state $|\alpha\rangle$ and the qubit is in a superposition state $(|g\rangle + |e\rangle)/\sqrt{2}$, i.e

$$|\psi(0)\rangle = \frac{(|g\rangle + |e\rangle)}{\sqrt{2}} |\alpha\rangle \quad (3.63)$$

we can apply the unitary time evolution operator on this state and use the following relation

$$e^{i\varphi \hat{n}} |\alpha\rangle = \sum_{n=0}^{\infty} \frac{\alpha^n e^{i\varphi n}}{\sqrt{n!}} e^{-\frac{|\alpha|^2}{2}} |n\rangle = |\alpha e^{i\varphi}\rangle \quad (3.64)$$

to get

$$\begin{aligned} |\psi(t)\rangle &= \hat{U}(t) |\psi(0)\rangle \\ &= \exp\left(-j\hat{\mathcal{H}}_0 t/\hbar\right) \frac{1}{\sqrt{2}} \left[e^{-j\varphi/2} |g\rangle |\alpha e^{-j\varphi}\rangle + e^{j\varphi/2} |e\rangle |\alpha e^{j\varphi}\rangle \right] \end{aligned} \quad (3.65)$$

where $\varphi = g^2 t / \Delta$. We can see that the cavity and qubit states are now entangled. The qubit ground state is entangled with the coherent state rotated by an angle $-\varphi$ and the excited state is entangled with the coherent state rotated by an angle φ .

At low powers, dispersive measurement is QND or Quantum Non-Demolition, which means that the qubit will remain in the eigenstate that was measured after a measurement. This means that repeated measurements will yield the same results.

3.9 Decoherence

A qubit which is initially in a superposition state $|\psi\rangle = \alpha|g\rangle + \beta|e\rangle$ will not stay in the superposition forever. It will lose its quantum information stochastically at a rate described below. The time for which the qubit retains its quantum information is called "coherence time", and is denoted by T_2 . There are 2 processes which cause decoherence [10].

- **Relaxation** The decay of the qubit to the ground state $|g\rangle$ due to spontaneous emission is referred to as relaxation. It does this at a rate Γ_{\downarrow} . If the qubit is in contact with a thermal bath at non zero temperature, there will also be excitation processes at a rate Γ_{\uparrow} . The combined effect gives the relaxation time $T_1 = (\Gamma_{\downarrow} + \Gamma_{\uparrow})^{-1}$. Relaxation processes can be attributed to phenomena that cause energy fluctuations.
- **Dephasing** Dephasing is the process by which the qubit loses its phase information due to fluctuations in qubit frequency. These fluctuations cause the qubit to gain or lose phase and on average, lead to a diffused phase.

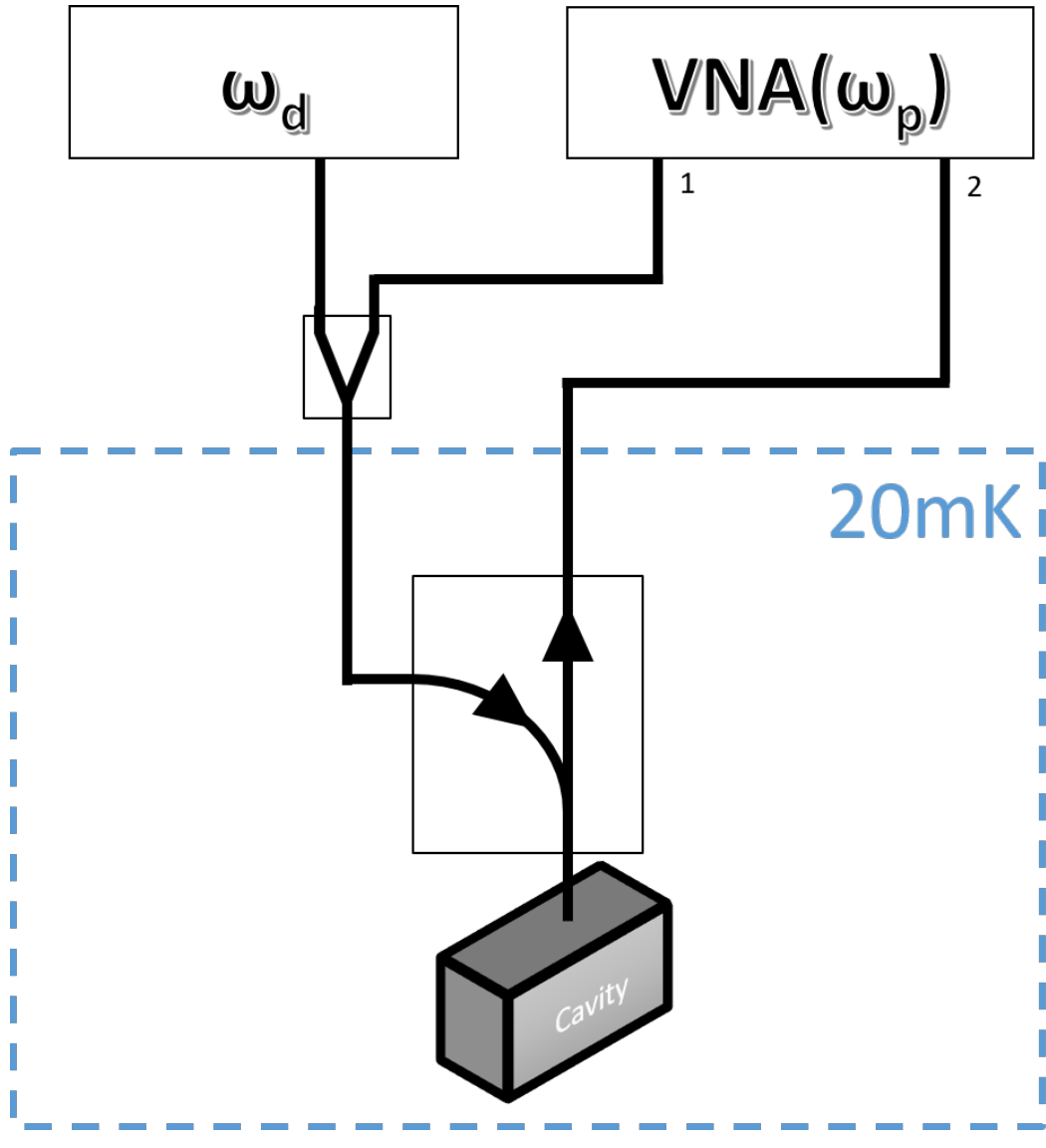


FIGURE 3.11: Measurement Setup. The probe signal from the VNA and the drive signal from the signal generator is combined using a power combiner.

3.10 Measurement Theory (Dispersive Limit)

The setup for measurements is shown in Fig. 3.11. All measurements described here assume that the cavity is dispersively coupled with the qubit. A signal of frequency ω_p is generated from port 1 of the VNA. This signal will be referred to as the probe signal. Another signal of frequency ω_d is combined with the probe signal and is sent into the cavity. This second signal is the drive signal. The VNA records the signal at port 2.

3.10.1 Single tone measurement

In this measurement the drive signal is switched off and only the probe signal is sent to the cavity. We can plot the amplitude as a function of power and frequency of this signal. During this measurement, the qubit remains in the ground state except at high powers. This measurement was performed in [15] with a 3D Transmon. The result of this measurement is similar to the ground state measurement in [17].

If the qubit is excited with a π -pulse at every point (i.e. for each frequency and power) and the amplitude is recorded for a certain period of time (≈ 400 ns) and averaged, we can see the response of both the ground state and excited states. This experiment was performed in [17] with a 2D Transmon.

- **Low Power Measurement**

The resonance occurs at the dispersively shifted frequency for low powers as expected.

- **High Power Measurement**

At high powers, the resonance shifts toward the bare cavity frequency. This is described as a bright state of the cavity and is discussed in [3]. The specific case of the transmon is discussed in [5] where the transmon is treated as a Multi Level System.

3.10.2 Two tone measurement

Both the probe signal and drive signal are applied continuously in this measurement. The probe frequency is close to the cavity frequency and is used to populate the cavity with photons. The drive frequency is close to the qubit frequency and is used to manipulate the qubit. Application of the drive frequency exactly at the qubit frequency will cause the qubit to leave the ground state. If this drive tone is applied continuously, the qubit will have an equal probability of being in the ground and excited state, so there will be no dispersive shift.

Varying the frequencies and powers of the two signals can produce useful results.

- By probing the cavity with a fixed low power and a frequency equal to the cavity frequency, while varying the frequency of the drive signal at constant

power, we can see a phase shift in the signal when the drive tone is at the qubit first transition frequency (ω_{01}). For larger powers of the drive signal, the phase shift is larger. At sufficiently large powers, we can also see the qubit transition to the second excited level at ω_{12} .

- If the drive signal is swept at a constant power and the probe power is increased, we can see the qubit frequency changing as a result of ac-Stark shift as the number of photons in the cavity increase.
- If the probe frequency is fixed close to the dispersively shifted resonance corresponding to one of the qubit states with a strong coupling rate and parameters such that $2\chi > \gamma, \kappa$, then spectroscopy with the drive frequency reveals the photon number state distribution in the cavity with different peaks corresponding to each photon number state. This is due to ac-Stark shift and is demonstrated using a Cooper Pair Box in [20].

Details about Time Domain Measurements can be found in Appendix-B

Appendix A

Calculation of Required Junction Resistance

If the capacitive pads of the transmon have a 70fF shunt capacitance (C_s)¹ as in [15], then the charging energy is

$$\frac{E_C}{h} = \frac{e^2}{2C_\Sigma} = \frac{e^2}{2 * 70 \text{ fF}} = 0.277\,056 \text{ GHz} \quad (\text{A.1})$$

To construct a 7 GHz qubit, $E_2 - E_1 = \sqrt{8E_J E_C} - E_C = h7 \text{ GHz}$. Then the Junction energy is

$$\frac{E_J}{h} = \frac{(h \times 7 \text{ GHz} + E_C)^2}{8E_C} = 23.89 \text{ GHz} \quad (\text{A.2})$$

The critical current for a given E_J can be calculated using 3.20.

$$I_0 = \frac{2eE_J}{\hbar} = 46.2442 \text{ nA} \quad (\text{A.3})$$

The Junction Resistance (R_N) can be calculated using the Ambegaokar-Baratoff formula

$$I_0 = \frac{\pi\Delta_s}{2eR_N} \tanh \frac{\Delta_s}{2k_B T} \quad (\text{A.4})$$

¹The shunt capacitance C_s is also the dominating capacitance for a junction with small area ($C_s \gg C_j$)

where k_B is the Boltzmann Constant and Δ_s is the superconducting gap, which in this case is that of aluminium. This can be calculated using BCS theory as

$$\Delta_s = 1.764 \times k_B T_C \quad (\text{A.5})$$

where $T_C = 1.1$ K si the critical temperature of aluminium.

In the zero temperature limit, the junction resistance R_N is given by

$$R_N = \frac{\pi \Delta_s}{2eI_0} = 5.681\,88 \text{ k}\Omega \quad (\text{A.6})$$

The junction inductance can also be calculated as

$$L_J = \frac{\Phi_0}{I_0} = \frac{\hbar}{2eI_0} = 7.098\,33 \text{ nH} \quad (\text{A.7})$$

Appendix B

Time Domain Measurements

The time domain measurements involve recording the reflected probe signal of the probe signal which is used to populate the cavity with photons.

The drive signal or control signal of frequency equal to the qubit frequency will be sent in pulses in order to manipulate the qubit.

The Measurement tone is sent and it's quadrature components are recorded continuously as a function of time. The method of measurement is well described and demonstrated in [2].

- **Cavity Decay Time (Ring-Down Measurement)**

This measurement involves sending a microwave pulse to populate the cavity with photons, and then measure the cavity response as a function of time. This is a ring down measurement since it involves the cavity losing photons and coming down to the zero-photon¹ state. The cavity response shows an exponential decay, and the time taken for the response to reduce by a factor of $1/e$ is the cavity decay time $1/\kappa$.

- **Rabi Measurement**

This measurement is used to calibrate the length of a π -pulse. The qubit is initialized in ground state². A pulse of length $\Delta\tau$ and frequency ω_q is sent to the cavity and then the cavity response is measured (ring-down for example)³.

This measurement is repeated multiple times and the average is taken. The

¹This refers to the experiment done at milli-Kelvin temperatures. Ring down measurement can also be done at higher temperatures, where the photon number comes down to thermal equilibrium

²This is done by waiting long enough so the qubit relaxes to ground state.

³A continuous measurement scheme is described in [2]

area between the measured curve (IQ values) for an arbitrary state and the ground state is proportional to the excitation probability of the qubit.

Plotting the excitation probabilities as a function of $\Delta\tau$ shows an oscillating behaviour. The pulse time for a π -pulse, which is $\Delta\tau$ for which the first peak in excitation probability is observed, is calibrated using this measurement.

- **Energy Relaxation Time T_1**

The experiment for finding the relaxation time T_1 for the qubit involves first exciting the qubit using a π -pulse, and measuring the cavity response after waiting for a time Δt . Plotting the excited state probability vs Δt shows an exponential decay. The time Δt at which the excitation probability drops to $1/e$ of the initial probability is the relaxation time T_1 .

- **Transverse Relaxation Time T_2**

The Ramsey Experiment is used to fin T_2 . It involves exciting the qubit to the superposition state $(|0\rangle + |1\rangle)/\sqrt{2}$ using a $\pi/2$ -pulse, and letting it evolve freely for a time $\Delta\tau$. After $\Delta\tau$ time, another $\pi/2$ -pulse is sent and the excitation probability is measured. This plot shows an exponential decay which gives T_2 at a decay of $1/e$.

Bibliography

- [1] Markus Aspelmeyer, Tobias J Kippenberg, and Florian Marquardt. "Cavity optomechanics". In: *Reviews of Modern Physics* 86.4 (2014), p. 1391.
- [2] R Bianchetti et al. "Dynamics of dispersive single-qubit readout in circuit quantum electrodynamics". In: *Physical Review A* 80.4 (2009), p. 043840.
- [3] Lev S Bishop, Eran Ginossar, and SM Girvin. "Response of the strongly driven Jaynes-Cummings oscillator". In: *Physical review letters* 105.10 (2010), p. 100505.
- [4] Alexandre Blais et al. "Cavity quantum electrodynamics for superconducting electrical circuits: An architecture for quantum computation". In: *Physical Review A* 69.6 (2004), p. 062320.
- [5] Maxime Boissonneault, JM Gambetta, and Alexandre Blais. "Improved superconducting qubit readout by qubit-induced nonlinearities". In: *Physical review letters* 105.10 (2010), p. 100504.
- [6] Audrey Cottet. "Implementation of a quantum bit in a superconducting circuit". PhD thesis. PhD Thesis, Université Paris 6, 2002.
- [7] Michel H Devoret et al. "Quantum fluctuations in electrical circuits". In: *Les Houches, Session LXIII* 7.8 (1995).
- [8] Richard P Feynman et al. *The feynman lectures on physics, vol. 3: Quantum mechanics*. 1966.
- [9] Jiansong Gao et al. "Noise properties of superconducting coplanar waveguide microwave resonators". In: *Applied Physics Letters* 90.10 (2007), p. 102507.
- [10] Kurtis Lee Geerlings. *Improving coherence of superconducting qubits and resonators*. 2013.
- [11] Roy J Glauber. "Coherent and incoherent states of the radiation field". In: *Physical Review* 131.6 (1963), p. 2766.

- [12] C Harmans. "Mesoscopic Physics: An Introduction". In: *Delft University* (1997).
- [13] JR Johansson, PD Nation, and Franco Nori. "QuTiP: An open-source Python framework for the dynamics of open quantum systems". In: *Computer Physics Communications* 183.8 (2012), pp. 1760–1772.
- [14] Jens Koch et al. "Charge-insensitive qubit design derived from the Cooper pair box". In: *Physical Review A* 76.4 (2007), p. 042319.
- [15] Hanhee Paik et al. "Observation of high coherence in Josephson junction qubits measured in a three-dimensional circuit QED architecture". In: *Physical Review Letters* 107.24 (2011), p. 240501.
- [16] David M Pozar. *Microwave engineering*. John Wiley & Sons, 2009.
- [17] MD Reed et al. "High-fidelity readout in circuit quantum electrodynamics using the Jaynes-Cummings nonlinearity". In: *Physical review letters* 105.17 (2010), p. 173601.
- [18] Susanne Richer and Barbara M Terhal. "Perturbative analysis of two-qubit gates on transmon qubits". PhD thesis. Master's thesis, RWTH Aachen, 2013.
- [19] David Isaac Schuster. *Circuit quantum electrodynamics*. 2007.
- [20] DI Schuster et al. "Resolving photon number states in a superconducting circuit". In: *Nature* 445.7127 (2007), pp. 515–518.